FINAL REPORT OF "ASSESSMENT OF MOLECULAR INTERACTIONS BETWEEN TUMOR CELL-DERIVED EXOSOMES AND THE TUMOR MICROENVIRONMENT"

Year 1. Descriptive analysis of Melanoma Cell Derived Exosomes

AIM 1. To explore the composition and complexity of Melanoma Cell Derived Exosome (MCDE) proteome and the miRNA assortment of MCDE.

AIM 1/TASK A. Proteomics

AIM 1/TASK B. Genomics

1.1. Isolation and characterization of exosomes

First, by adapting the protocol of Peinado et al. (Peidano et al., 2012), we isolated extracellular vesicles from B16F1 mouse melanoma cells which fit to the exosome size range (30-120 nm). As was shown by employing SEM and AFM (Figure 1A and B), the isolated fraction indeed contained exosomes as the particles were cap-shaped and their size was within the 40-70 nm range. Then, existence of those molecules was assessed by Western blotting which are characteristics of exosomes (Yáñez-Móet al., 2015; Lötvall et al., 2014); as shown in Figure 1C, the exosome-size nanosomes indeed expressed the exosome markers CD9, CD63, CD81 and Hsp70.

Exosomes were then subjected to large-scale analysis to determine their protein and miRNA profiles. Whole proteome analysis (using LC-MSMS technology) and the corresponding bioinformatics methods (identification of elements of the exosome's proteomics spectrum in the UniProt data base and comparison of the resulted findings with elements of the ExoCarta data base) revealed that the 95 distinct proteins identified in the melanoma-derived exosomes (their list can be found in Table 1) exhibited an 86.3% overlap with those molecules which are listed as characteristic exosome protein markers in the ExoCarta data base. Further, miRNA sequencing (using SOLiD 5500 technology) identified 168 known miRNA elements (Table 2) which, similar to the proteomics data, exhibited a large (93.5%) overlap with those molecules which are listed as characteristic exosome miRNA markers in the ExoCarta data base.

To uncover the functional significance of the proteomics and miRNA sequencing data, the Ingenuity Pathway Analysis (IPA) technology was employed. This bioinformatics analysis defined that the identified proteins most probably participate in such cell and molecular processes as "Cell Death and Survival", "Cellular Movement", "Cell-to-Cell Signaling and Interaction", "Cellular Growth and Proliferation" and "Cell Morphology" ($P_{range}=7.53*10^{-15}$ – $9.32*10^{-4}$ significance range) (Figure 1D). Very similar to these data, functions of the identified miRNAs are suggested to be linked to mechanisms of "Cellular Development", "Cellular Growth and Proliferation", "Cellular Movement", "Cell Cycle" and "Cell Death and Proliferation" ($P_{range}=1.25*10^{-12}$ – $4.88*10^{-2}$ significance range) (Figure 1E).

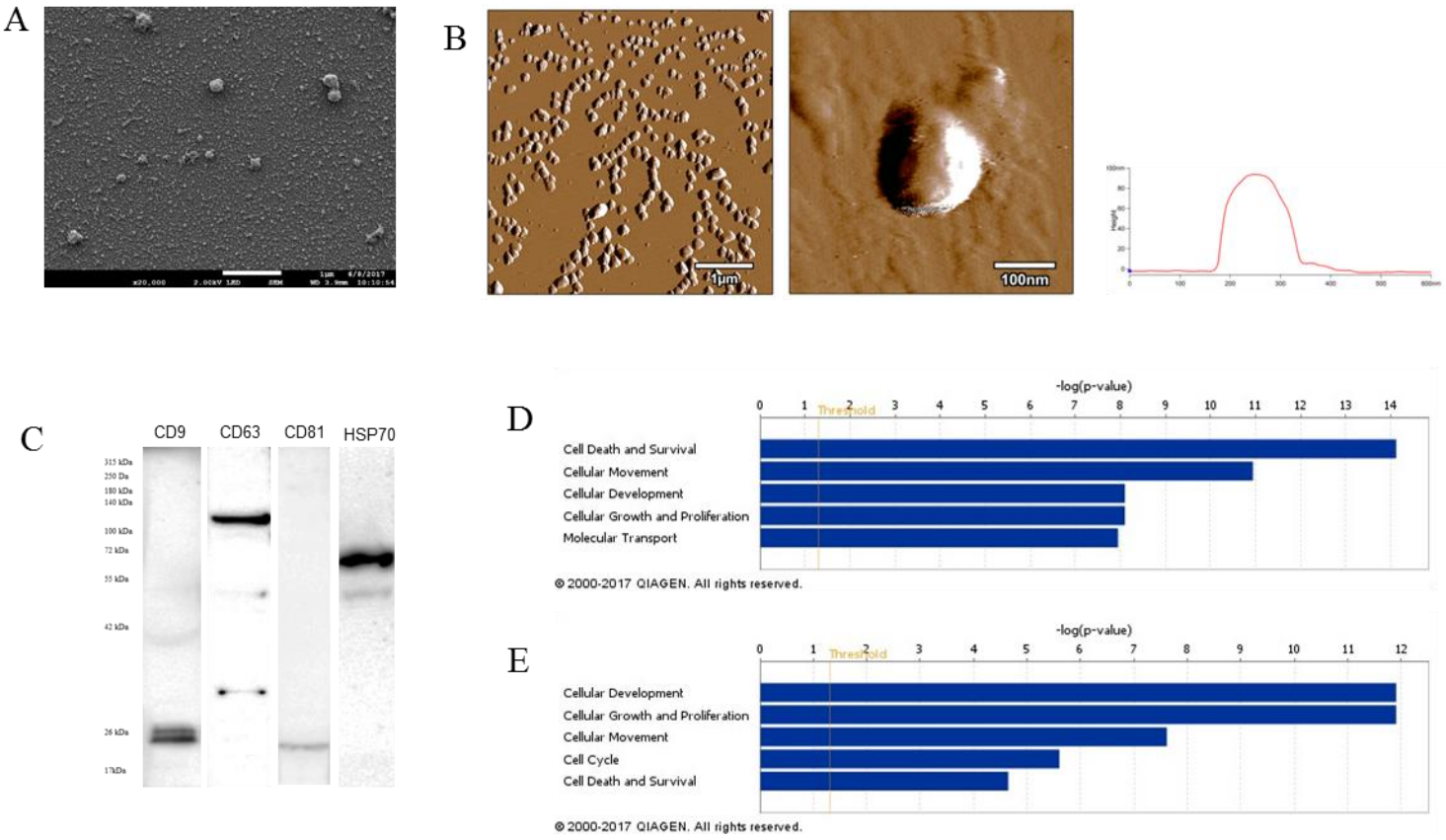

Figure 1. Characterization of B16F1 melanoma cell culture-derived exosomes

(A) Scanning electron mirograph of exosomes.

(B) Atomic force microscopy images of exosomes. Left and middle pictures represent the shape and surface topography of vesicles, right graph represents height profile.

(C) Western blot analysis of common exosome markers (CD9, CD63, CD81, HSP70).

(D and E) Top 5 molecular and cellular functions identified by Ingenuity Pathway Analysis (IPA) of exosomal proteins and miRNAs.

Table 1. List of exosomal proteins identified by LC-MSMS

ID	Symbol	Entrez Gene Name
P97857	ADAMTS1	ADAM metallopeptidase with thrombospondin type 1 motif 1
Q3TNX8	ADAMTS4	ADAM metallopeptidase with thrombospondin type 1 motif 4
Q640N1	AEBP1	AE binding protein 1
P05064	ALDOA	aldolase, fructose-bisphosphate A
P97429	ANXA4	annexin A4
P48036	ANXA5	annexin A5
P08226	APOE	apolipoprotein E
Q3TWT5	ASAH1	N-acylsphingosine amidohydrolase 1
Q3TXF9	ATP1A1	ATPase Na+/K+ transporting subunit alpha 1
P97370	ATP1B3	ATPase Na+/K+ transporting subunit beta 3
Q1XID4	ATP6AP2	ATPase H+ transporting accessory protein 2
Q9JL18	BACE2	beta-site APP-cleaving enzyme 2
O55107	BSG	basigin (Ok blood group)
Q8R2Q8	Bst2	bone marrow stromal cell antigen 2
Q9WVT6	CA14	carbonic anhydrase 14
P41731	CD63	CD63 molecule
P35762	CD81	CD81 molecule
P10605	CTSB	cathepsin B
P18242	CTSD	cathepsin D
P29812	DCT	dopachrome tautomerase
P57776	EEF1D	eukaryotic translation elongation factor 1 delta
Q3UAM9	ENG	endoglin
P17182	ENO1	enolase 1
P19096	FASN	fatty acid synthase
P30416	FKBP4	FK506 binding protein 4
P11276	FN1	fibronectin 1
P09528	FTH1	ferritin heavy chain 1
P16858	GAPDH	glyceraldehyde-3-phosphate dehydrogenase
P08752	GNAI2	G protein subunit alpha i2
Q3TAV1	GPNMB	glycoprotein nmb
P19157	GSTP1	glutathione S-transferase pi 1
P11499	HSP90AB1	heat shock protein 90 alpha family class B member 1
B1B0C7	HSPG2	heparan sulfate proteoglycan 2
Q9CQW9	IFITM3	interferon induced transmembrane protein 3
G3UYZ1	IGSF8	immunoglobulin superfamily member 8
Q91VK4	ITM2C	integral membrane protein 2C
P02468	LAMC1	laminin subunit gamma 1
Q60961	LAPTM4A	lysosomal protein transmembrane 4 alpha
P35951	LDLR	low density lipoprotein receptor
Q07797	LGALS3BP	galectin 3 binding protein
Q3U2W5	LGALS8	galectin 8
P16056	MET	MET proto-oncogene, receptor tyrosine kinase
P21956	MFGE8	milk fat globule-EGF factor 8 protein
Q2TA50	MLANA	melan-A
Q6NVG5	MREG	melanoregulin
Q9EPX2	PAPLN	papilin, proteoglycan like sulfated glycoprotein
Q3UIP2	PCOLCE	procollagen C-endopeptidase enhancer
Q80Y09	PDCD6IP	programmed cell death 6 interacting protein
P62962	PFN1	profilin 1
P09411	PGK1	phosphoglycerate kinase 1
P52480	PKM	pyruvate kinase, muscle
Q9CZB2	PMEL	premelanosome protein
P17742	PPIA	peptidylprolyl isomerase A
P35700	PRDX1	peroxiredoxin 1
Q61171	PRDX2	peroxiredoxin 2
Q543S0	PRELP	proline and arginine rich end leucine rich repeat protein
P53994	RAB2A	RAB2A, member RAS oncogene family
Q8CCG5	RALB	RAS like proto-oncogene B
O89086	RBM3	RNA binding motif (RNP1, RRM) protein 3
P35980	RPL18	ribosomal protein L18
Q3U5P4	SCPEP1	serine carboxypeptidase 1
O08992	SDCBP	syndecan binding protein
Q0VGP2	SEMA3B	semaphorin 3B
P32261	SERPINC1	serpin family C member 1
P10852	SLC3A2	solute carrier family 3 member 2
Q3UQM7	SLC7A5	solute carrier family 7 member 5
O09044	SNAP23	synaptosome associated protein 23
Q64337	SQSTM1	sequestosome 1
Q8CI59	STEAP3	STEAP3 metalloreductase
Q3TDG9	STX12	syntaxin 12
O70439	STX7	syntaxin 7
P40749	SYT4	synaptotagmin 4
O88968	TCN2	transcobalamin 2
Q542D9	TFRC	transferrin receptor
P39876	TIMP3	TIMP metallopeptidase inhibitor 3
Q4FJX7	TINAGL1	tubulointerstitial nephritis antigen like 1
Q9DCS1	TMEM176A	transmembrane protein 176A
Q9R1Q6	TMEM176B	transmembrane protein 176B
Q9CZX7	TMEM55A	transmembrane protein 55A
Q9QY73	TMEM59	transmembrane protein 59
O88746	TOM1	target of myb1 membrane trafficking protein
O89023	TPP1	tripeptidyl peptidase 1
Q3UCW0	TSG101	tumor susceptibility 101
Q4FJW7	TSPAN4	tetraspanin 4
Q8BJU2	TSPAN9	tetraspanin 9
P11344	TYR	tyrosinase
P07147	TYRP1	tyrosinase related protein 1
O70404	VAMP8	vesicle associated membrane protein 8
Q8R0J7	VPS37B	VPS37B, ESCRT-I subunit
Q8R105	VPS37C	VPS37C, ESCRT-I subunit
O88384	VTI1B	vesicle transport through interaction with t-SNAREs 1B
A8DUQ1	HBBT1	beta-globin
P70356	MELA	Gag-pol poliprotein
P70355	MELA	envelope protein
Q811J2	LOC72520	LOC72520 protein

Table 2. List of exosomal miRNAs identified by SOLiD 5500xl technology

Symbol	Seed regio	ID
let-7a-3p	UAUACAA	mmu-let-7a-1-3p
		mmu-let-7b-3p
		mmu-let-7c-2-3p
		mmu-let-7f-1-3p
let-7a-5p	GAGGUAG	mmu-let-7a-5p
		mmu-let-7b-5p
		mmu-let-7c-5p
		mmu-let-7d-5p
		mmu-let-7e-5p
		mmu-let-7f-5p
		mmu-let-7g-5p
		mmu-mir-98-5p
let-7d-3p	UAUACGA	mmu-let-7d-3p
let-7i-3p	UGCGCAA	mmu-let-7i-3p
miR-100-5p	ACCCGUA	mmu-mir-99a-5p
		mmu-mir-99b-5p
miR-101-3p	ACAGUAC	mmu-mir-101a-3p
miR-103-1-5p	GCUUCUU	mmu-mir-107-5p
miR-103-3p	GCAGCAU	mmu-mir-103-3p
		mmu-mir-107-3p
miR-10a-5p	ACCCUGU	mmu-mir-10a-5p
		mmu-mir-10b-5p
miR-1191a	AGUCUUA	mmu-mir-1191a
miR-1249-3p	CGCCCUU	mmu-mir-1249-3p
miR-125b-5p	CCCUGAG	mmu-mir-125a-5p
		mmu-mir-125b-5p
		mmu-mir-351-5p
miR-126a-5p	AUUAUUA	mmu-mir-126a-5p
miR-128-3p	CACAGUG	mmu-mir-128-3p
miR-129-1-3p	AGCCCUU	mmu-mir-129-1-3p
		mmu-mir-129-2-3p
miR-129b-5p	CUUUUUG	mmu-mir-129b-5p
miR-130a-3p	AGUGCAA	mmu-mir-130a-3p
		mmu-mir-130b-3p
		mmu-mir-301a-3p
		mmu-mir-301b-3p
miR-130a-5p	CUCUUUU	mmu-mir-130a-5p
miR-130b-5p	CUCUUUC	mmu-mir-130b-5p
miR-132-3p	AACAGUC	mmu-mir-132-3p
miR-132-5p	ACCGUGG	mmu-mir-132-5p
miR-135a-5p	AUGGCUU	mmu-mir-135a-5p
miR-138-5p	GCUGGUG	mmu-mir-138-5p
miR-139-5p	CUACAGU	mmu-mir-139-5p
miR-140-3p	ACCACAG	mmu-mir-140-3p
miR-140-5p	AGUGGUU	mmu-mir-140-5p
miR-142-3p	GUAGUGU	mmu-mir-142a-3p
		mmu-mir-143-5p
miR-144-3p	ACAGUAU	mmu-mir-144-3p
miR-144-5p	GAUAUC	mmu-mir-144-5p
miR-145-5p	UCCAGUU	mmu-mir-145a-5p
miR-146a-5p	GAGAACU	mmu-mir-146a-5p
miR-148a-3p	CAGUGCA	mmu-mir-148b-3p
		mmu-mir-152-3p
miR-151-3p	UAGACUG	mmu-mir-151-3p
miR-15a-3p	AGGCCAU	mmu-mir-15a-3p
miR-15b-3p	GAAUCAU	mmu-mir-15b-3p
miR-16-2-3p	CCAAUAU	mmu-mir-16-2-3p
miR-16-5p	AGCAGCA	mmu-mir-15a-5p
		mmu-mir-15b-5p
		mmu-mir-16-5p
		mmu-mir-195a-5p
		mmu-mir-322-5p
		mmu-mir-497a-5p
miR-17-3p	CUGCAGU	mmu-mir-17-3p
miR-17-5p	AAAGUGC	mmu-mir-106b-5p
		mmu-mir-17-5p
		mmu-mir-20a-5p
		mmu-mir-93-5p
miR-181a-1-3p	CCAUCGA	mmu-mir-181a-1-3p
miR-181a-5p	ACAUUCA	mmu-mir-181a-5p
		mmu-mir-181b-5p
		mmu-mir-181c-5p
		mmu-mir-181d-5p
miR-1827	GAGGCAG	mmu-mir-709
miR-1839-3p	GACCUAC	mmu-mir-1839-3p
miR-185-5p	GGAGAGA	mmu-mir-185-5p
miR-186-5p	AAAGAAU	mmu-mir-186-5p
miR-187-3p	CGUGUCU	mmu-mir-187-3p
miR-188-3p	UCCCACA	mmu-mir-188-3p
miR-188-5p	AUCCCUU	mmu-mir-188-5p
miR-18a-5p	AAGGUGC	mmu-mir-18a-5p
miR-191-5p	AACGGAA	mmu-mir-191-5p
miR-193a-3p	ACUGGCC	mmu-mir-193a-3p
miR-1981-3p	AUCUAAC	mmu-mir-1981-3p

Symbol	Seed regio	ID
miR-199a-3p	CAGUAGU	mmu-mir-199a-3p
		mmu-mir-199b-3p
miR-199a-5p	CCAGUGU	mmu-mir-199a-5p
		mmu-mir-199b-5p
miR-19b-3p	GUGCAAA	mmu-mir-19a-3p
		mmu-mir-19b-3p
miR-204-5p	UCCCUUU	mmu-mir-211-5p
miR-21-5p	AGCUUAU	mmu-mir-21a-5p
miR-210-3p	UGUGCGU	mmu-mir-210-3p
miR-210-5p	GCCACUG	mmu-mir-210-5p
miR-219a-5p	GAUUGUC	mmu-mir-219a-5p
miR-22-3p	AGCUGCC	mmu-mir-22-3p
miR-22-5p	GUUCUUC	mmu-mir-22-5p
miR-221-3p	GCUACAU	mmu-mir-222-3p
miR-223-3p	GUCAGUU	mmu-mir-223-3p
miR-224-5p	AAGUCAC	mmu-mir-224-5p
miR-23a-3p	UCACAUU	mmu-mir-23a-3p
		mmu-mir-23b-3p
miR-24-1-5p	UGCCUAC	mmu-mir-24-2-5p
miR-24-3p	GGCUCAG	mmu-mir-24-3p
miR-26a-5p	UCAAGUA	mmu-mir-26a-5p
		mmu-mir-26b-5p
miR-27a-3p	UCACAGU	mmu-mir-27a-3p
		mmu-mir-27b-3p
miR-29a-5p	CUGAUUU	mmu-mir-29a-5p
miR-29b-1-5p	CUGGUUU	mmu-mir-29b-1-5p
miR-29b-3p	AGCACCA	mmu-mir-29a-3p
		mmu-mir-29b-3p
		mmu-mir-29c-3p
miR-3065-5p	CAACAAA	mmu-mir-3065-5p
miR-30c-5p	GUAAACA	mmu-mir-30a-5p
		mmu-mir-30b-5p
		mmu-mir-30c-5p
		mmu-mir-30d-5p
		mmu-mir-30e-5p
miR-31-3p	GCUAUGC	mmu-mir-31-3p
miR-31-5p	GGCAAGA	mmu-mir-31-5p
miR-3176	CUGGCCU	mmu-mir-378d
miR-324-5p	GCAUCCC	mmu-mir-324-5p
miR-328-3p	UGGCCCU	mmu-mir-328-3p
miR-329-3p	ACACACC	mmu-mir-362-3p
miR-33-5p	UGCAUUG	mmu-mir-33-5p
miR-330-5p	CUCUGGG	mmu-mir-326-3p
miR-331-3p	CCCCUGG	mmu-mir-331-3p
miR-339-5p	CCCUGUC	mmu-mir-339-5p
miR-340-3p	CCGUCUC	mmu-mir-340-3p
miR-344a-5p	CAGGCUC	mmu-mir-484
miR-345-5p	CUGACCC	mmu-mir-345-5p
miR-3473b	GGCUGGA	mmu-mir-3473b
		mmu-mir-3473e
miR-34a-5p	GGCAGUG	mmu-mir-34a-5p
		mmu-mir-34b-5p
		mmu-mir-34c-5p
miR-34c-3p	AUCACUA	mmu-mir-34b-3p
miR-350	UCACAAA	mmu-mir-350-3p
miR-361-5p	UAUCAGA	mmu-mir-361-5p
miR-362-5p	AUCCUUG	mmu-mir-362-5p
miR-374b-5p	UAUAAUA	mmu-mir-374b-5p
miR-378a-3p	CUGGACU	mmu-mir-378a-3p
		mmu-mir-378c
miR-378a-5p	UCCUGAC	mmu-mir-378a-5p
miR-3909	GUCCUCU	mmu-mir-877-3p
miR-423-3p	GCUCGGU	mmu-mir-423-3p
miR-423-5p	GAGGGGC	mmu-mir-423-5p
miR-425-5p	AUGACAC	mmu-mir-425-5p
miR-451a	AACCGUU	mmu-mir-451a
miR-501-5p	AUCCUUU	mmu-mir-501-5p
miR-503-5p	AGCAGCG	mmu-mir-503-5p
miR-532-5p	AUGCCUU	mmu-mir-532-5p
miR-542-3p	GUGACAG	mmu-mir-542-3p
miR-574-5p	GAGUGUG	mmu-mir-574-5p
miR-582-5p	UACAGUU	mmu-mir-582-5p
miR-652-3p	AUGGCGC	mmu-mir-652-3p
miR-670-5p	UCCCUGA	mmu-mir-670-5p
miR-700-5p	AAGGCUC	mmu-mir-700-5p
miR-744-3p	UGUUGCC	mmu-mir-744-3p
miR-744-5p		mmu-mir-744-5p
miR-7a-5p	GGAAGAC	mmu-mir-7a-5p
miR-872-3p	GAACUAU	mmu-mir-872-3p
miR-872-5p	AGGUUAC	mmu-mir-872-5p
miR-9-5p	CUUUGGU	mmu-mir-9-5p
miR-92a-3p	AUUGCAC	mmu-mir-25-3p
		mmu-mir-32-5p
		mmu-mir-92a-3p

AIM2. Inhibition of cell proliferation. Comparison of the miRNA and protein content of MCDE before and after treatment with a classical and a non-conventional cytostatic agent.

AIM2/TASK A: Melanoma cells will be treated with doxorubicin hydrochloride, a classical chemotherapeutic agent.

AIM2/TASK B: B16F1 melanoma cell culture will be treated with Ag-TiO2-induced by 305 nm light.

1.2. Treatment of cells and differences of exosomes

In the first step we optimized the cytostatic treatments on 5-8F nasopharyngeal carcinoma and B16F1 melanoma cells by a proliferation assay. Doxorubicin and $AgTiO_2$ was used at a concentration of 0.6 μM and 2.5 μg/ml, respectively. The photoreactive $AgTiO_2$ nanoparticles were induced by a low-pressure mercury lamp mostly emitting light wavelength λ≥360 nm, for 60 min from a 10 cm distance in the culture medium. Exosomes were isolated after a 72h incubation period and analysed by quantitative and qualitative methods.

1.2.1. Characterization of 5-8F cell-derived exosomes

The quantity of produced exosomes was analysed by nanoparticle tracking analysis (Nanosight NS500 device) and showed significant changes after the treatments (Figure 2).

In the case of the 5-8F human nasopharyngeal carcinoma cells, the qualitative analysis of exosome content targeted the miRNAs. The SOLiD 5500xl technology and the bioinformatics supported the high-quality screening of miRNA content. miRNA diversity impressively increased after treatments. In the control samples 71 different types of miRNA were identified. This increased to 121 types in the doxorubicin-treated samples and to 223 in the $AgTiO_2$-treated ones. Other quantitative miRNA changes and literature data are summarized in Table 3. Based on this table, we hypothesized, that nasopharyngeal carcinoma cells release tumor suppressor miRNAs via exosomes and retain the oncogenic and resistance-enhancing ones under stress to maintain their tumorigenecity. In contrast, under normal conditions, cells produce and release miRNA types that promote progression and metastasis formation *in vivo*.

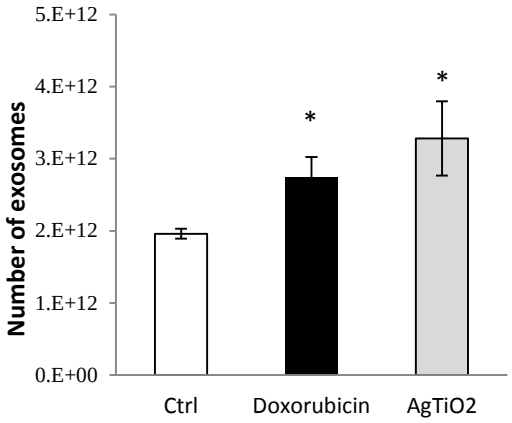

Figure 2. NanoSight analysis of 5-8F exosome samples.

$AgTiO_2$ treatment resulted in a remarkably increased exosome production of 5-8F cells (p= 0.0023). Similarly, doxorubicin resulted in significantly (p=0.001) elevated exosome production.

Table 3. Normalized expression values of miRNAs and their previously described oncogenic potential in cancer

miRNA	Ctrl	Doxo	Ag-TiO_2	miRNAs previously described				
				cancer type	specimen	effect	targets	ref
mir-205	217933	92055	213069	NPC	clinical specimens and cell lines: CNE2, 6-10B and 9-4E	O	TP53INP1	(T1)
				NPC	cell lines: CNE-2R, CNE-2	O	PTEN	(T2)
let-7b	108344	43337	52824	NPC	cell lines: HK1, HONE1, NP69, NP460	TS	c-Myc	(T3)
mir-21	48568	156766	52607	NPC	clinical samples and cell lines: CNE-1, CNE-2, TWO3 and C666-1	O	PTEN	(T4)
					clinical samples and NPC cell line	O	BCL2	(T5)
					NP69. C666-1, CNE2, HONE1, 6-10B Akata(+), Akata(-), Ramos, Namalwa, Raji, B95-8	O	PDCD4, Fas-L	(T6)
mir-339	28643	1916	4188	BC	clinical samples and cell lines: MCF-7, MDA-MB-231, MDA-MB-468	TS	BCL-6	(T7)
				CRC	clinical samples and cell lines: HCT116, HT29, LS174T, SW480, SW620, LOVO	TS	PRL-1	(T8)
				NSCLC	clinical samples and cell lines: 95D, 95C	TS	BCL-6, VCP	(T9)
mir-4286	23661	737	325	GBM	clinical samples and cell lines: U-87 MG, U-118 MG, LN18	NA	C2ORF21, LRRC4, VAMP1, ERO1L, PDE4A	(T10)
mir-1260a	17435	0	631	NBL	cell line: SH-SY5Y, animal model	O	ADAMTS-1 and CREB	(T11)
mir-324	17435	1253	453	glioma	cell lines: U87, LN229	TS	GLI1	(T12)
mir-93	17435	5675	625	NPC	clinical samples and cell lines: CNE1, CNE2	O	TGFβR2	(T13)
mir-1260b	11208	0	108	PC	clinical samples and cell line: PC-3	O	sFRP1, Smad4	(T14)
mir-33b	11208	811	752	CRC	clinical samples and cell lines: HT-29, HCT 116, SW480	TS	CDK6, CCND1,Pim-1	(T15)
				OSA	clinical samples and cell lines: MG-63, U2OS, SOSP-9607, SAOS-2	TS	c-Myc	(T16)
mir-423	11208	1916	982	HCC	cell lines: HEK-293T, HepG2	O	p21Cip1/Waf1	(T17)
mir-532	11208	1032	5214	MM	clinical samples and cell lines: M1-M11	O	RUNX3	(T18)
mir-4284	9963	5528	172	GBM	GBM neurosphere cultures and U87 cell line	TS		(T19)
mir-99b	7472	369	7764	HNSCC	meta-analysis and cell lines: 1386Ln, UM1	TS	IGF1R	(T20)
				NSCLC	clinical samples and cell lines: H1299, H522, HCC95, HCC1438	TSr	FGFR3	(T21)
				PC	clinical samples and cell lines: LNCaP, C4-2, and WPE1-NB26	TS	SMARCA5, SMARCD1, mTOR.	(T22)
mir-1307	6227	0	3149	CRC	clinical samples and cell lines: Caco-2, CHO, DLD-1, HCT116, LoVo, and SW620	O	Bcl2	(T23)
mir-451a	6227	7886	57356	NPC	clinical samples and cell lines: NP69 CNE-1, CNE-2, C666-1, HNE-1, HONE-1, SUNE-1, 5-8 F, and 6-10B	TS	MIF	(T24)
				HSCC	clinical samples and cell lines: FaDu, SAS	TS	ESDN	(T25)
mir-33a	3736	442	153	LC	cell lines: A549, H1299, BEAS-2B, NCI-H460, HOS	TS	PTHrP	(T26)
mir-130b	3736	1032	115	CRC	clinical samples and cell line: CHO	O	PTEN	(T27)
				GC	clinical samples and cell lines: AGS, SNU1, SNU5, SNU16, AZ521, MKN7, MKN28, MKN45	O	RUNX3	(T28)
				PC	clinical samples and cell lines: ANC-1, ASPC-1, Miapaca-2, BXPC-3, SW1990	TS	STAT3	(T29)
let-7f-1	2491	42821	6189	NPC	cell lines: HK1, HONE1, NP69, NP460	TS	c-Myc	(T3)
mir-16-1	2491	11940	24822	NPC	cell line: CNE-2Z	TS	Bcl2	(T30)
				NPC	cell lines: BL41, BL41/B95.8, Jijoye, EREB2.5	TS	BRCA-1	(T31)
let-7f-2	1245	43485	6196	NPC	cell lines: HK1, HONE1, NP69, NP460	TS	c-Myc	(T3)
mir-16-2	1245	11498	24586	NPC	cell line: CNE-2Z	TS	Bcl2	(T30)
				NPC	cell lines: BL41, BL41/B95.8, Jijoye, EREB2.5	TS	BRCA-1	(T31)
mir-186	0	32650	6980	BCA	clinical samples and cell lines: J82, HT1376, RT4, T24 and TCCSUP HCV29	TS	NSBP1	(T32)
				NSCLC	clinical samples and cell lines: A549, NCI-H358, H157, H1299, 16HBE	TS	ROCK1	(T33)
mir-15a	0	19679	14750	NPC	cell line: CNE-2Z	TS	Bcl2	(T30)
				NPC	cell lines: BL41, BL41/B95.8, Jijoye, EREB2.5	TS	BRCA-1	(T31)
mir-26b	0	15920	2486	NPC	cell line: 293	TS	COX-2	(T34)
let-7e	0	10540	2033	NPC	cell lines: HK1, HONE1, NP69, NP460	TS	c-Myc	(T3)
mir-224	0	7591	14266	NSCLC	clinical samples and cell lines: H1299, H3122, H2228, A549	O	TNFAIP1, SMAD4	(T35)
				ESCC	clinical samples and cell lines: TE13, Eca109	O	PHLPP1 PHLPP2	(T36)
mir-31	0	6412	15388	NPC	cell lines: C666-1, NP69	TS	FIH1, MCM2	(T37)
mir-590	0	1695	6699	NPC	clinical samples and cell lines:CNE1, CNE2, C666-1	TS	CD44	(T38)

NPC: nasopharyngeal carcinoma, O: oncogene, TS: tumor suppressor, BC: breast cancer, CRC: colorectal cancer, NSCLC: non-small cell lung cancer, GBM: glioblastoma, NBL: neuroblastoma, PC: prostate cancer, OSA: osteosarcoma, HCC: hepatocellular carcinoma, MM: malignant melanoma, HNSCC: head and neck squamous cell carcinoma, HSCC: hypopharyngeal squamous cell carcinoma, LC: lung cancer, GC: gastric cancer, BCA: bladder cancer, ESCC: oesophageal squamous cell carcinoma

1.2.2. Characterization of B16F1 cell-derived exosomes

In the case of B16F1 mouse melanoma cells, we used an additional treatment also, a 42 °C heat shock, which is not a cytostatic agent, but another type of stress condition for the cells. Quantitative analysis of exosomes showed decrease of vesicle production after doxorubicin treatment, but a significant increase ($p=0.012$) was observed after $AgTiO_2$ treatment (Figure 3A-B).

The qualitative analysis of exosome samples targeted the miRNAs and proteins. miRNA content and whole proteome of exosomes were analyzed by SOLiD 5500xl technology and mass spectrometry (LC-MSMS on LTQ Orbitrap Elite [Thermo] mass spectrometer), respectively. Altogether 172 type of miRNAs and 216 different proteins were detected in the exosomes. However these molecules showed extremely different distribution in each exosome sample (Figure 3C-F).

Functional analysis of the miRNA and proteomic data was performed by the DIANA-mirPath and the Ingenuity Pathway Analysis (IPA) software, respectively. Analysing the top 3 overexpressed miRNAs in each exosome sample revealed that the cells release many miRNAs, which affect many tumor-related pathways in the recipient cells (Table 4).

Analysing the whole proteome of exosome samples revealed that stress conditions caused significant changes in several signal pathways, including some cancer-related ones (Figure 3G). In the case of doxorubicin and heat stress, analysis of exosomal proteomic data predicted activation of the biological function 'growth of tumor' and inhibition of majority of biological functions related to cell movement. $AgTiO_2$ did not cause any significant changes in these functions (Figure 3H-I).

Table 4. The most significant targeted pathways by the top 3 overexpressed miRNAs

	p value		
KEGG pathway	**Doxorubicin**	**Heat stress**	**$AgTiO_2$**
TNF signaling pathway	5.01E-04	1.29E-02	1.30E-02
Proteoglycans in cancer	5.01E-04	2.20E-02	3.66E-05
mTOR signaling pathway	4.53E-03	N/A	1.93E-02
MAPK signaling pathway	8.80E-05	N/A	4.28E-02
Cell cycle	N/A	1.29E-02	4.80E-03

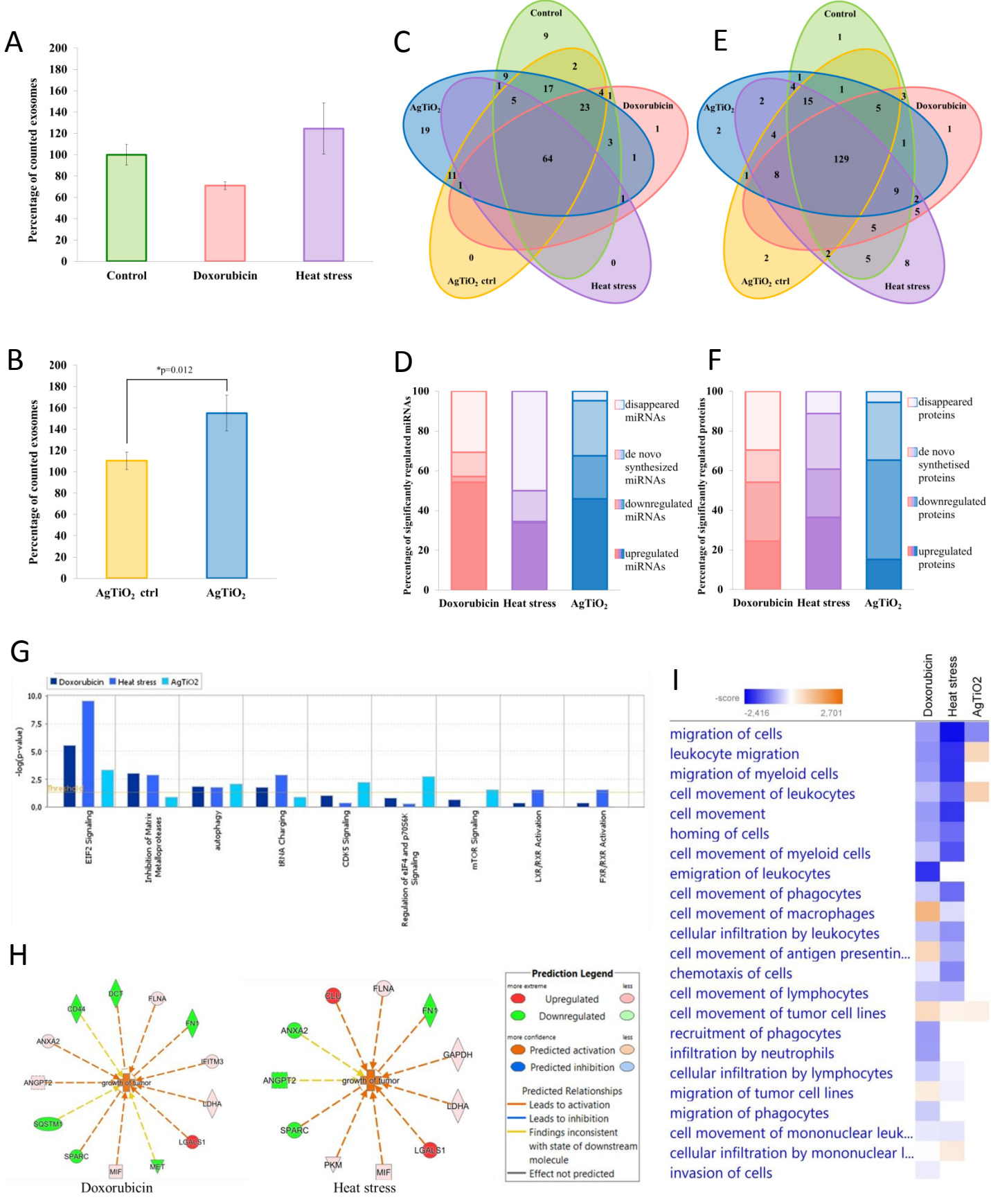

Figure 3. Descriptive analysis of stress conditioned B16F1 cell-derived exosomes

(A-B) NanoSight analysis of exosome samples.

(C-D) miRNA profile of exosomes.

(E-F) proteome profile of exosomes

(G) Significantly regulated tumor-related pathways (IPA analysis).

(H) Proteins, which influence the biological function named"growth of tumor" (IPA analysis).

(I) Changes of cell movement-related biological functions (IPA analysis).

Planned dissemination of results 1.

"We plan to develop a protocol for exosome production and purification for own use and for future scientific collaboration. Our results will be presented at least at 1 national and 1 international scientific meeting as oral presentation. At the end of the 1st year we will complete one in extenso publicationfor an internationally referred scientific journal."

Accomplished dissemination of results 1.

In the 1st year we participated in publishing a review and presented our results in 1 international and 1 national conference. We had 3 other publications also.

Publications:

1. Yáñez-Mó M, Siljander PR-M, Andreu Z, Buzas K et al. Biological properties of extracellular vesicles and their physiological functions. Journal of Extracellular Vesicles. 2015;4:10.3402/jev.v4.27066. doi:10.3402/jev.v4.27066.

Other publications:

1. Farkas, B; Zsedenyi, A; Gyukity-Sebestyen, E; Romano, I; Nagy, K; Diaspro, A; Brandi F; Buzas, K; Beke, S: Excimer Laser-produced Biodegradable Photopolymer Scaffolds Do Not Induce Immune Rejection In Vivo, JOURNAL OF LASER MICRO NANOENGINEERING, 2015
2. Lesjak M, Simin N, Orcic D, Franciskovic M, Knezevic P, Beara I, Aleksic V, Svircev E, Buzas K, Mimica-Dukic N: Binary and Tertiary Mixtures of Satureja hortensis and Origanum vulgare Essential Oils as Potent Antimicrobial Agents Against Helicobacter pylori., Phytotherapy Research, 2015
3. Buzas K, Kiss A, Vizler C. Current approaches of tumor immunotherapy. ACTA BIOLOGICA SZEGEDIENSIS 59:(Suppl 1) pp. 69-82. (2015)

Oral presentations:

1. Edina Gyukity-Sebestyen, Maria Harmati, Gabriella Dobra, Annamaria Marton, Robert L. Katona, Peter Horvath, Istvan Nagy, Csaba Vizler, Katalin Medzihradszky, Eva Hunyadi-Gulyas, Sandor Kormondi and Krisztina Buzas. Melanoma cell-derived exosomes alter the microenviroment of malignant tumours via re-education of mesenchymal stem cells by miRNAs. 4th Annual Meeting of the International Society for Extracellular Vesicles, Washigton, USA, 2015.04.23 26.
2. Edina Gyukity-Sebestyen, Maria Harmati, Gabriella Dobra, Annamaria Marton, Robert L. Katona, Peter Horváth, Istvan Nagy, Csaba Vizler, Katalin Medzihradszky, Eva Hunyadi-Gulyas, Sandor Kormondi, Istvan Nemeth, Tamas Biro, Krisztina Buzas. Interaction between melanoma exosomes and mesenchymal stem cells induce cancer stem cell generation and progression of metastatic disease. Magyar Imunnológiai Társaság 44. Vándorgyűlése, Velence, 2015.10.14-16.

Poster presentations:

1. Maria Harmati, Edina Gyukity-Sebestyen, Gabriella Dobra, Okay Saydam, Laszlo Janovak, Imre Dekany, Gabor Decsi, Sandor Kormondi, Zsofia Tarnai, Anna Farago, Katalin Nagy, Krisztina Buzas. Cell damage results altered exosome profile of nasopharyngeal carcinoma cells. 4th Annual Meeting of the International Society for Extracellular Vesicles, Washigton, USA, 2015.04.23-26.

Year 2. Investigation of alterations in cell physiology induced by Melanoma Cell Derived Exosomes

AIM 3: Phenotyping of MSCsTo follow phenotypic changes of MSCs after MCDE induction by FACS.

AIM 4: Apoptotic responses

AIM 6: Histone acetylation

2.1. *In vitro* effects of exosomes on MSC populations

We then investigated the effects of exosomes on biological processes (e.g. proliferation, survival, malignant transformation, etc.) of MSCs which are generally considered as proper *in vitro* models of tumor stroma (Karnoub et al., 2007). For these experiments, MSC cultures were initiated from mouse abdominal adipose tissue (Liu et al., 2012) and were subjected to melanoma-derived exosome treatment.

First, we assessed whether exosomes are internalized by MSCs. High-throughput microscopy showed that the MSCs (labeled green by the $DiOC_{18}(3)$ lipid dye) indeed uptake the exosomes (labeled red by the $DiIC_{18}(3)$ lipid dye) as soon as 1-2 hrs after application. Importantly, after 24 hrs, the majority of MSC are loaded by the exosomes (Figure 4A and B); indeed, statistical analysis revealed a 91% internalization efficacy. This suggests that the below functional alterations are due to cell-population, and not to individual cell, level effects induced by the exosome treatment.

We then determined whether the internalized exosomes induced a melanoma-like malignant transformation of the MSCs. By employing two complementary cell counting methods, we found that proliferation rate of the MSCs significantly accelerated 24 hrs after exosome exposure (Figure 4C). By flow cytometry, we also showed that the exosome-treated MSC exhibited a partial resistance to the cell death-inducing effects of 100 ng/ml tumor necrosis factor-α (TNFα) as, in these cultures, the fraction of the dead cells is significantly decreased (Figure 4D).

Since the exosomes were isolated from melanoma cells, we were then intrigued to uncover whether the above alterations (which all argue for the malignant transformation of the susceptible cells) also resulted in the *de novo* appearance of melanoma-specific features in the transformed MSCs. To answer this question, expressions of melanoma-specific markers, MlanA and MITF, were investigated. By Q-PCR, we found that mRNA transcript levels of both markers markedly elevated in the MSCs upon exosome treatment (Figure 4E), albeit the kinetics of elevation of the 2 molecules were slightly different. Moreover, in good accord with the mRNA data, immunofluorescent labeling showed that oncosome exposure markedly increased the expression of MlanA at the protein level as well (Figure 4F).

2.2. Exosome exposition resulted in an oncogenic reprogramming of MSCs *in vitro*

Next, we assessed whether the above effects of exosomes to induce malignant-like transformation of the MSCs is accompanied by a cellular-molecular oncogenic reprogramming of the target cells. Naive MSCs were exposed to a standardized volume of exosomes for various time intervals (to avoid the experimental fluctuations we collected pooled samples from multiple independent *in vitro* experiments, see Methods section) and then samples were subjected to Q-PCR analysis by using a self-designed panel of 40 oncogenes and tumor suppressor genes which were previously suggested to play a putative role in melanoma progression (Table 5).

As shown in Figure 5A, gene expression pattern of MSCs exposed to melanoma-derived exosomes exhibited a clear oncogenic dominance (compared to the non-exposed cell). This is verified by statistical analysis of the averaged relative gene expression levels of all molecules investigated which revealed statistically higher values in the exosome treated cells ($p=1.9x10^{-5}$, $p=0.031$, $p=2.3x10^{-8}$ for the 6, 24 and 72 hrs time point, respectively).

Kleffel et al. has recently shown that melanoma cell subpopulations which overexpress PD-1, quite intriguingly, exhibit remarkably increased invasiveness and aggressive growth properties (Kleffel S, 2015). However, they did not define the factor(s) which induce(s) the above PD-1 overexpression. Since the above finding strongly suggested the "MSC re-education" capacity of melanoma-derived exosomes to induce malignant-like behavior, we next assessed the expression of PD-1 in the MSC cultures.

As expected, only insignificant PD-1 expression (both at the mRNA and protein levels) could be identified in control, non-treated MSCs. In contrast, a marked, significant, and time-dependent elevation of PD-1 upon exosome treatment was detected by Q-PCR (Figure 5B) and by complementary Western blot and immunofluorescent labeling techniques (Figure 5C and D). Further, by employing super-resolution microscopy, we were able to identify the dramatic upregulation of PD-1 at the single molecular level in the exosome-treated MSCs (Figure 5E).

Importantly, since proteomics analysis did not identify the presence of PD-1 in the exosomes, these data suggest that the high PD-1 protein content in exosome-exposed MSCs was a result of *de novo* induction and not of exosome-mediated molecular transfer. Our finding therefore suggest that melanoma-derived exosome-mediated "re-education" of the cells resulted in a novel MSC population which could be labelled as $MSC^{PD\text{-}1+}$.

To determine the global histone post-translational changes following exosome treatment we tested the H3K4me3, H3K14ac and H4K5ac levels as an active chromatin mark. In addition, we measured the heterochromatin related H3K9me3 mark as repressive mark. An imbalance in the equilibrium of histone H3 and H4 acetylation has been associated with tumorigenesis and cancer progression. As we expected we could detect increase in H3K4me and H3K14ac which suggest transcriptional reprogramming. In accordance the level of S2 and S5 phosphorylated RNAPII also increased suggesting an exosome mediated global transcriptional change. In contrary the H3K9me3 decrease and increase in H4K5ac also suggest a global chromatin structural change which is often associated with cancerous malformations (Figure 6).

Finally we investigated the uptake by MSCs of stress conditioned B16F1 cell-dervied exosomes also and we observed that the kinetics of exosome uptake is different in each case (Figure 7).

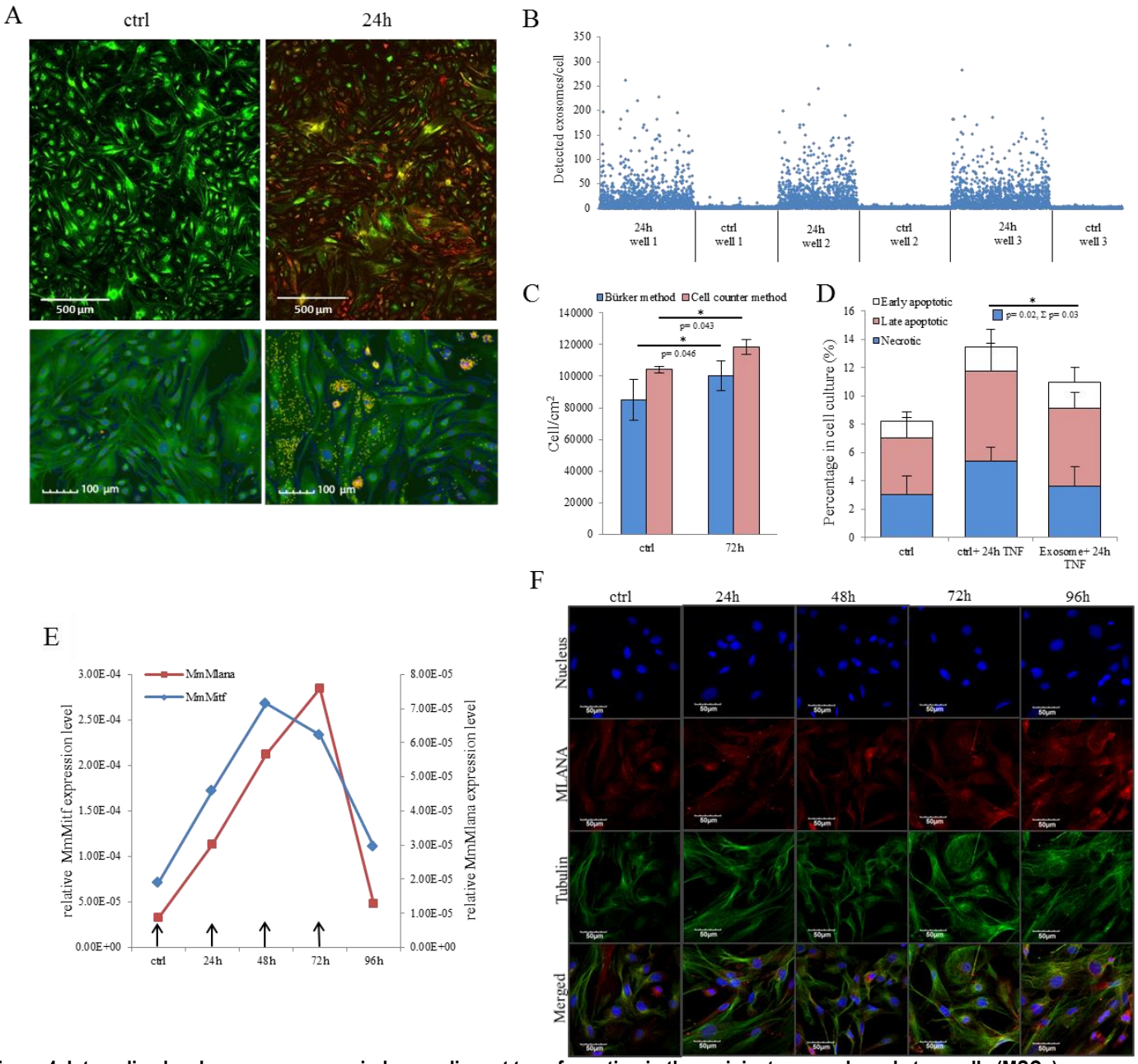

Figure 4. Internalised melanoma exosomes induce malignant transformation in the recipient mesenchymal stem cells (MSCs)

(A) Fluorescent images of exosome uptake by MSCs. DiO (green fluorescent lipid dye)-labeled cells were exposed to DiL (red fluorescent lipid dye)-labeled exosomes for 24h and fixed in 4% PFA. Control cells were treated in the same manner without exosomes. Pictures were aquired by the Operetta high content screening system (Perkin Elmer). Lower 2 images represent an experiment, where nuclei were counterstained with DAPI and the exosomes were detected with a customized version of A-trous wavelet transform, and highlighted with yellow.

(B) Quantitative analysis of exosome uptake. The graph shows the number of detected exosomes (Y axis) in each cell (X axis) in 3 exosome-exposed (24h) and 3 control cell cultures (ctrl).

(C) Cell proliferation assay of exosome-exposed MSCs. Cells were plated at the same density of $1*10^4$ cell/cm^2 for the control and the exosome-exposed cultures as well, and 72h after the exosome treatment the cell number was determined by manual counting and automated cell counter. Both method showed significantly increased cell proliferation of exosome-treated cells. Results are presented as mean ± SD (n=3).

(D) Apoptosis analysis of exosome-exposed MSCs by flow cytometry. Exosome-pre-exposed cells were treated by 100 ng/ml TNFα for 24h, stained with Annexin V-FITC and proidium iodide and analysed by flow cytometry along with a TNFα-treated and an untreated control cell culture. The graph represents the percentage of early apoptotic, late apoptotic and necrotic cells. TNFα-induced total cell death and necrosis also were significantly lower (Σp=0.03 and p=0.02, respectively) in the exosome-pretreated cell cultures compared to the corresponding control cells. Results are presented as mean + SD (n=3).

(E) qRT-PCR analysis of MlanA and Mitf in MSC cultures treated by exosomes in every 24h as arrows indicate on the graph. The expression of both mRNA increased after the exosome exposition, but they showed different kinetics.

(F) Fluorescent immunocytochemistry of MlanA in exosome-exposed MSC cultures using a primary rabbit antibody to MlanA and a secondary AlexaFluor555-conjugated antibody to rabbit IgG (red). α-tubulin network of cells was directly labeled by an AlexaFluor488-conjugated antibody (green) and the nuclei were stained with DAPI (blue).

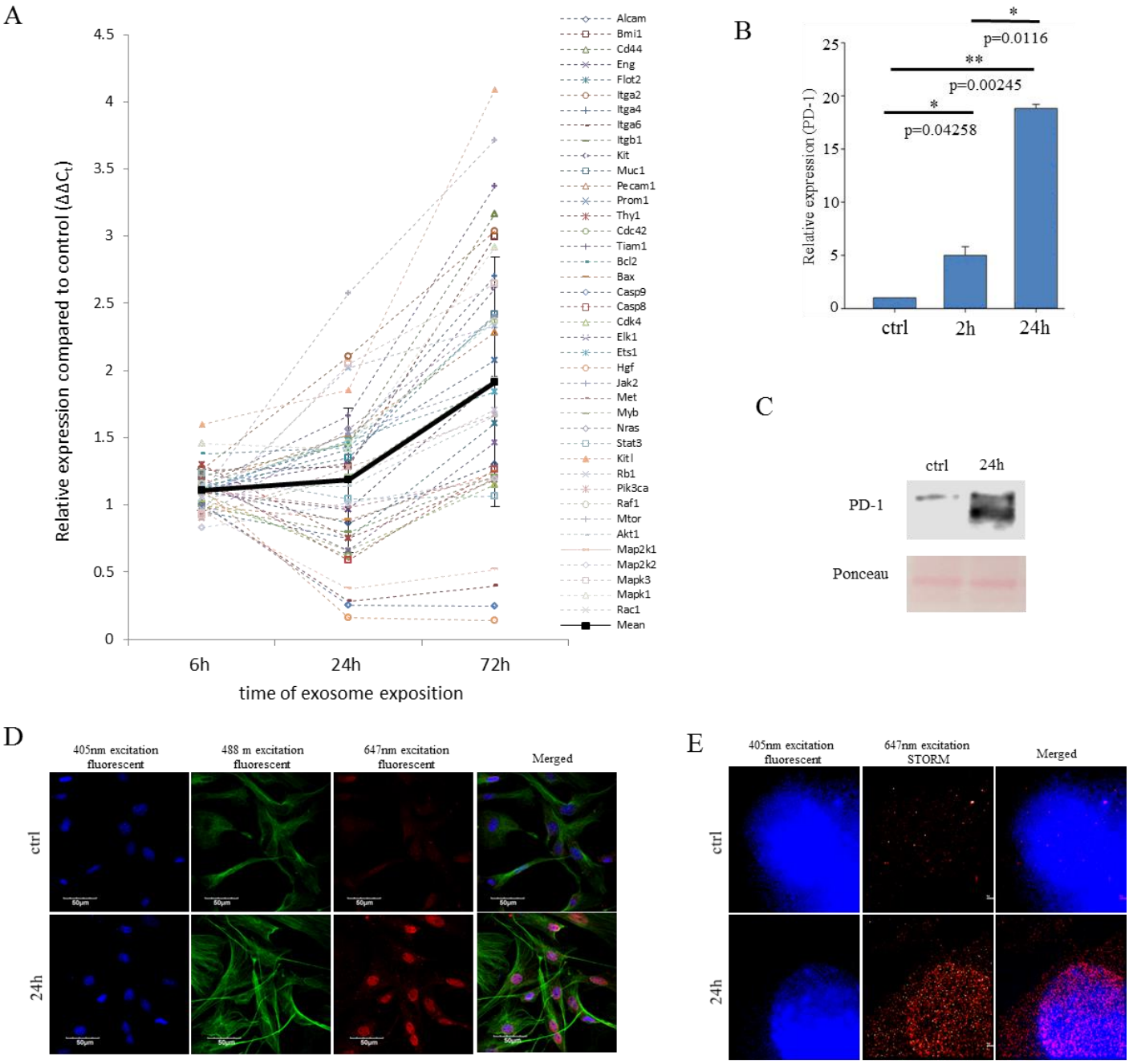

Figure 5. Exosome-reeducated MSCs show oncogene dominance and PD-1 expression.

(A) qRT-PCR analysis of 40 tumor-related genes (listed in Table 5) in exosome-exposed MSCs using a self-designed panel. The graph shows the relative expression values for each gene after 6h, 24h and 72h of exosome exposition. The trendline of altered gene expression pattern (labeled by thick black line) shows an increasing tendency over time (mean ± SD).

(B) qRT-PCR analysis of PD-1 in MSCs after 2h and 24h of exosome exposition. The graph represents mean + SEM.

(C) Representative immunoblot of PD-1 protein expression in the control and exosome-exposed MSCs after 24h of exosome treatment.

(D-E) Fluorescent immunocytochemistry of PD-1 in 24h exosome-exposed MSC cultures using a primary rat antibody to PD-1 and a secondary AlexaFluor647-conjugated antibody to rat IgG (red). Nuclei were stained with DAPI. (D) α-tubulin network of cells was directly labeled by an AlexaFluor488-conjugated antibody (green). Images were aquired by confocal microscopy. (E) Images were taken by STORM super-resolution microscopy. STORM super-resolution imaging of PD-1 reveals that PD-1 is localized mostly around the nucleus, which are blurred and not resolvable using diffraction-limited confocal microscopy of the same region.

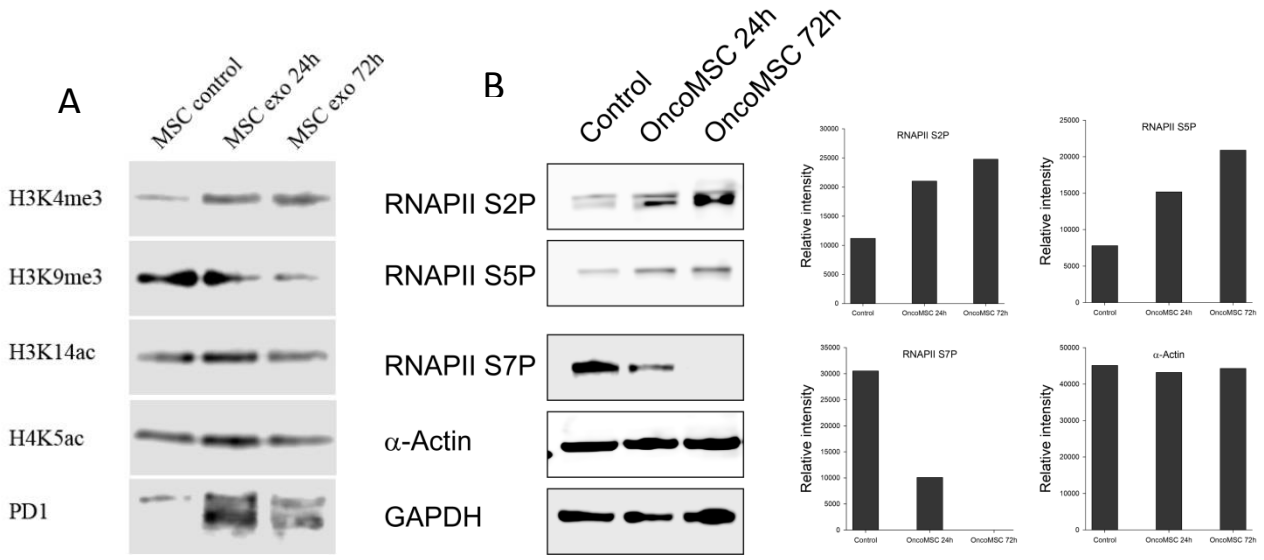

Figure 6. Exosome induced histone modifications and RNAPII phosphorylation changes in MSCs

(A) Westren blot analysis of histone post-translational modifications.

(B) Western blot analysis of phosphorylational changes of RNAPII.

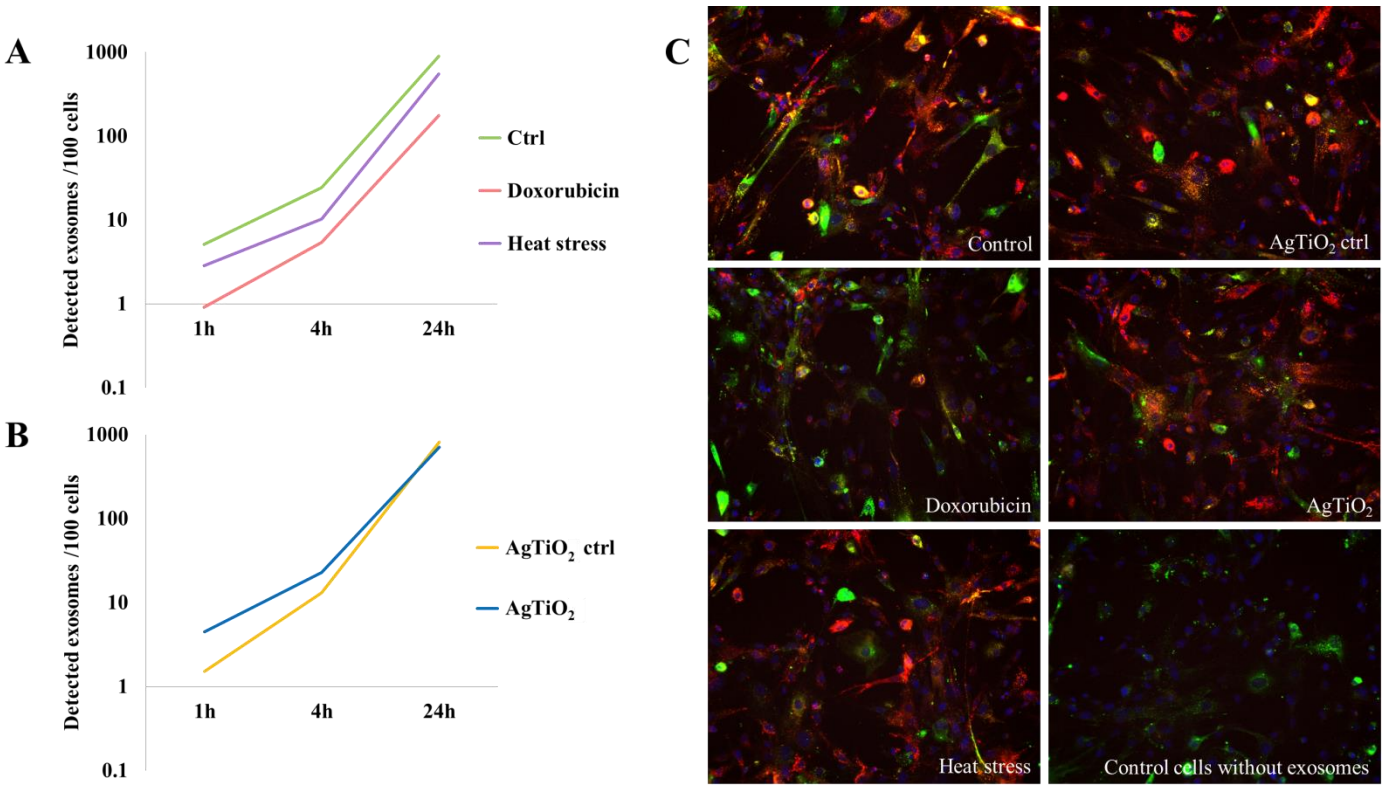

Figure 7. Kinetics of stress conditioned B16F1 cell-derived exosome uptake by MSCs.

(A-B) Average exosome number in 100 cells after 1, 4 and 24h incubation.

(A) Representative images of exosome uptake after 24h incubation. Cells and exosomes were labeled by green lipid dye (DiO) and red lipid dye (DiL), respectively.

Table 5. List of genes investigated by a self-designed oncopanel

Gene	Protein	Function	Ref.
Alcam	ALCAM (CD166) Activated leukocyte cell adhesion molecule	plays an important role in human malignant melanoma progression and formation of locoregional and distant metastases.	(Piotr Donizy, 2016)
Bmi1	BMI1 B cell-specific Moloney murine leukemia virus integration site 1	induces an invasive signature in melanoma that promotes metastasis and chemoresistance	(Roberta Ferretti, 2016)
Cd44	CD44	CD44s interaction with HA plays a crucial role in cell invasiveness	(Mummert ME, 2003)
Eng	Endoglin (CD105)	has a crucial role in angiogenesis, important protein for tumor growth, survival and metastasis of cancer cells to other locations in the body.	(Raquel Mun˜oz, 2013)
Flot2	Flotillin-2	is associated with melanoma progression	(Hazarika P, 2004)
Itga2	ITGA2 Integrin alpha2	was associated with increased risk of melanoma	(Lenci RE,2011)
Itga4	ITGA4 Integrin alpha 4	α4β1 integrin plays an important role in metastasis of malignant melanoma	(Silke Kuphal, 2005)
Itga6	ITGA6 Integrin alpha 6	α6β1 integrin as a laminin receptor expression is associated with invasive potential in a highly metastatic melanoma cell line	(Shona R Elshaw, 2001)
Itgb1	ITGB1 Integrin beta-1 (CD29)	α4β1 integrin plays an important role in metastasis of malignant melanoma	(Silke Kuphal, 2005; Shona R Elshaw, 2001)
Kit	KIT (CD117)	c-Kit signaling activates the MAPK and PI3K signaling cascades	(Matteo S. Carlino, 2014)
Muc1	Mucin1	promotes melanoma migration through the Akt signaling pathway	(Xiaoli Wang, 2015)
Pecam1	Pecam1 (CD31)	could play multiple roles in diverse processes related to melanoma development, dormancy, migration/invasion and angiogenesis	(James M. Dunleavey, 2014)
Prom1	CD133	melanoma stem cell marker	(Madjd Z, 2016)
Thy	THY1 (CD90)	cell adhesion molecule. Melanoma cells use Thy-1 on endothelial cells for metastasis formation	(Schubert K, 2013)
Cdc42	CDC42 Cell division control protein 42 homolog	Cdc42 is vital for the transforming Ras signal emanating from endomembranes.	(Kristy Stengel, 2011)
Tiam1	Tiam1 T-cell lymphoma invasion and metastasis 1	have crucial roles in regulation of the actin cytoskeleton, cell migration, cell cycle progression, gene transcription and cell adhesion	(Meghan E. Minard, 2004)
Bcl2	Bcl-2 B-cell lymphoma 2	plays a pivotal role in the regulation of molecules associated with the migratory and invasive phenotype, contributing, in cooperation to hypoxia, to tumor progression	(Daniela Trisciuoglio, 2005)
Bax	Bcl-2-associated X protein	plays a crucial role in apoptotic cell death induced, the Bax/Bcl-2 ratio determines the susceptibility of melanoma cells	(Raisova M, 2001)
Casp9	Caspase-9	has been linked to the mitochondrial death pathway	(Raisova M, 2001)
Casp8	Caspase-8	plays a central role in the execution-phase of cell apoptosis	(Dwayne G. Stupack, 2013)
Cdk4	CDK4 Cyclin-dependent kinase 4	promote cell-cycle progression and inhibit both cell senescence and apoptosis	(Sheppard KE,2013)
Elk1	ELK1	member of ETS oncogene family, transcription activator	(Hamblin MR, 2016)
Ets1	ETS1 E26 transformation-specific	require for migration in cell lines with an active RAS/ERK signaling pathway	(Plotnik JP, 2014)
Hgf	HGF Hepatocyte growth factor	can activate the MAP-kinase pathway, which is upregulated in the majority of melanoma, through the proto-oncogene c-MET	(Hügel R, 2016)
Jak2	Janus kinase 2	activator of transcription (STAT) pathway is thought to play a central role in melanoma cell biology	(Nicholas C, 2011)
Met	MET Hepatocyte growth factor receptor	induces several biological responses that collectively give rise to a program known as invasive growth	Al-U'datt DG, 2017
Myb	MYB	Is a transcription factor. Among other genes, MYB regulates the transcription of the Kit, Bcl2, Ets-2 and N-Ras.	Ramsay RG, 2008
Nras	Neuroblastoma RAS viral oncogene homolog	Ras recruits and stimulates a number of intracellular signaling pathways including the Raf/MEK/ERK mitogen activated protein kinase (MAPK) pathway, the PI3K/AKT pathway	Fedorenko IV, 2013
Stat3	STAT3 Signal transducer and activator of transcription 3	promotes transcription of many genes that involve in melanoma metastasis	Cao HH, 2016
Kitl	KIT-ligand Stem cell factor (CD117)	is a cytokine that binds to the c-KIT receptor. This cytokine plays an important role in melanogenesis.	Matteo S. Carlino, 2014
Rb1	Retinoblastoma 1 protein	is a tumor suppressor protein that is dysfunctional in several major cancers	Roesch A, 2005
Pik3ca	PI3K	PI3K/AKT pathway play a pivotal role in tumor development, growth and metastasis of melanoma.	Livingstone E, 2014
Raf1	RAF1 Proto-oncogene serine/threonine-protein kinase	is a crucial regulators of the ERK MAP kinase signaling cascade	Kyriakis JM, 1992
Mtor	mTOR Mechanistic target of rapamycin	is a serine/threonine protein kinase that regulates cell growth, cell proliferation, cell motility, cell survival.	Caunt CJ, 2015
Akt1	AKT (Protein kinase B)	plays a key role in multiple cellular processes such as glucose metabolism, apoptosis, cell proliferation, transcription and cell migration.	Livingstone E, 2014
Map2k1	MEK1 Dual specificity mitogen-activated protein kinase kinase 1	is essential component of the MAP kinase signal transduction pathway, this kinase is involved in many cellular processes such as proliferation, differentiation, transcription regulation and development.	Caunt CJ, 2015
Map2k2	MEK2	play a critical role in mitogen growth factor signal transduction. It phosphorylates and thus activates MAPK1/ERK2 and MAPK2/ERK3.	Caunt CJ, 2015
Mapk3	ERK1 extracellular-signal-regulated kinases	Ras-Erk1/2 is a key regulator pathway in melanoma cell proliferation.	Caunt CJ, 2015
Mapk1	ERK2	Ras-Erk1/2 is a key regulator pathway in melanoma cell proliferation.	Caunt CJ, 2015
Rac1	RAC1		

Planned dissemination of results 2.

"We are going to present our data at 1 national and 1 international scientific conference. We will start to edit the second in extenso publication and analyze collected data to compare the physiological mechanisms and measurable conditions."

Accomplished dissemination of results 2

In the 2nd year we presented our results in 1 international and 1 national conference. We had 3 publications in other topics.

Other publications:

1. Buzás K, Marton A, Vizler C, Gyukity-Sebestyén E, Harmati M, Nagy K, Zvara Á, Katona RL, Tubak V, Endrész V, Németh IB, Oláh J, Vígh L, Bíró T, Kemény L.: Bacterial sepsis increases survival in metastatic melanoma: Chlamydophila pneumoniae induces macrophage polarization and tumor regression., J Invest Dermatol. 2016 Apr;136(4):862-5.
2. Harmati M, Gyukity-Sebestyen E, Dobra G, Terhes G, Urban E, Decsi G, Mimica-Dukić N, Lesjak M, Simin N, Pap B, Nemeth IB, Buzas K.: Binary mixture of Satureja hortensis and Origanum vulgare subsp. hirtum essential oils: in vivo therapeutic efficiency against Helicobacter pylori infection., Epub 2016 Aug 31.
3. Marton A, Kúsz E, Kolozsi C, Tubak V, Zagotto G, Buzás K, Quintieri L, Vizler C.: Vanillin Analogues o-Vanillin and 2,4,6-Trihydroxybenzaldehyde Inhibit NFκB Activation and Suppress Growth of A375 Human Melanoma., Anticancer Res. 2016 Nov;36(11):5743-5750.,

Oral presentations:

1. Edina Gyukity-Sebestyén, Mária Harmati, Gabriella Dobra, Árpád Bálind, Johanna Mihály, Ágnes Zvara, Éva Hunyadi-Gulyás, Róbert Katona, István Nagy, István B. Németh, Lajos Kemény, Tamás Bíró, Krisztina Buzás. Intercellular communication between melanoma and stroma cells induce PD-1 expression and tumor progression. Magyar Imunnológiai Társaság 45. Vándorgyűlése, Velence, 2016.10.19-21.

Poster presentations:

1. Harmati M, Gyukity-Sebestyen E, Dobra G, Nagy I, Hunyadi-Gulyas E, Horvath P, Botyanszki B, Saydam O, Janovak L, Dekany I, Buzas K. Induced cell damage altered proteome and miRNA profile of melanoma exosomes and interactions with tumor stroma cells. 5th Annual Meeting of the International Society for Extracellular Vesicles, Rotterdam, Netherlands, 2016.05.04-07.
2. Dobra G, Harmati M, Gyukity-Sebestyen E, Tarnai Zs, Decsi G, Kormondi S, Szegletes Zs, Janovak L, Dekany I, Saydam O, Nagy I, Nagy K, Buzas K. Stressors alter intercellular communication and exosome profile in nasopharyngeal carcinoma cells. 5th Annual Meeting of the International Society for Extracellular Vesicles, Rotterdam, Netherlands, 2016.05.04-07.

Year 3 Investigation of in vivo effects of exosome treated MSCs in tumor bearing mice

AIM 7: To assess metastasis formation in tumor bearing mice injected with MCDE-treated MSCs.

3. *In vivo* findings

3.1. Oncosomes augment *in vivo* tumorigenesis and tumor progression

After presenting evidence on the *in vitro* tumorigenic induction potential of exosomes on cultured MSCs, we hypothesized that this phenomenon could be identified *in vivo* as well. To probe this assumption, we employed the well-known animal model, routinely used in our laboratories (Buzas K, 2016), in which tumors, developed mostly in the lungs, are induced in mice by the intravenous administration of mouse B16F1 melanoma cells (to the tail vein). Tumor-bearing mice received culturing media (control group), or exosomes isolated from the same B16F1 melanoma cells, or exosome-induced $MSC^{PD\text{-}1+}$ cells.

Notably, both the exosome and $MSC^{PD\text{-}1+}$ groups were characterized by a markedly increased size of the tumor-covered lung tissues (the increase proved to be significant in the $MSC^{PD\text{-}1+}$ group) (Figure 8A). Of further importance, we also found that, in both exosome groups, the number of distant metastases also significantly elevated when compared to the control (Figure 8B). As we have seen during our previous studies, these metastases were mostly localized to the ovaries and kidneys (and very rarely in the lymph nodes) of control tumor-bearing animals. However, besides these sites, the presence of exosomes resulted in frequent metastases in the lymph nodes and, as a new location, in the liver. Interestingly, in $MSC^{PD\text{-}1+}$ treated mice, the exosome-transformed MSCs could be identified in the para-aortic lymph nodes by FISH (Figure 8C) which verified the successful *in vivo* adherence of $MSC^{PD\text{-}1+}$cells.

3.2. Exosomes significantly alter gene expression profiles in lung tissues of tumor-bearing mice

Lung tissues of the different groups were then subjected to in-depth expressional profiling 14 days after injection of exosomes or $MSC^{PD\text{-}1+}$ cells. Namely, Q-PCR analysis was performed by using a self-designed panel of 40 genes; besides the housekeeping genes, we assessed expressions of those genes which are i) proto-oncogenes; ii) reportedly involved in malignant transformation; and/or iii) found to be involved in melanoma development and progression (Table 5).

Hierarchical cluster analysis (HCA) of the gene expression patterns clearly showed a robust proto-oncogenic dominance in lung samples of the exosome and $MSC^{PD\text{-}1+}$ groups when compared to the control tissues. Indeed, we identified significant *de novo* induction of 26 and 23 genes (Alcam1, Eng, Flot2, Itga4, Itga6, Kit, Pecam1, Prom1, Thy, Cdc42, Tiam1, Bcl2, Bax, Casp9, Casp8, Ets1, Hgf, Jak2, Met, Myb, Map2k1, Map2k2, Mapk1, Elk1, Rb1, Itga2) and (Alcam1, Eng, Flot2, Itga4, Itga6, Kit, Pecam1, Prom1, Thy, Cdc42, Tiam1, Bcl2, Bax, Casp9, Casp8, Ets1, Hgf, Jak2, Met, Myb, Map2k1, Map2k2, Mapk1), respectively, with at least 10 fold increase, and additional 6 genes in exosome induced group (Cd44, Itgb1, Muc1, Pik3ca, Akt1, Rac1) and 3 genes in $MSC^{PD\text{-}1+}$ group (Cd44, Itgb1, Rac1) with at least 2 fold mRNA level elevations (Bmi1, Cdk4, Stat3, Kitl, Raf1, Mtor) and (Bmi1, Muc1, Cdk4, Stat3, Kitl, Pik3ca, Mtor, Akt1), respectively (Figure 8D presents a heatmap of indicative data of overexpressed genes induced by exosome exposure).

We furthermore showed that, besides the above genes, expression of PD-1 was also significantly increased in both exosome groups (Figure 8E); notably, although the mRNA transcript level of PD-1 was close to double in $MSC^{PD\text{-}1+}$ lung tissues in comparison to the samples in the exosome group, the difference was not significant (most probably due to the large inter-animal variability and standard error).

We constructed a Venn-diagram (Figure 8F) to show all possible logical connections between the various gene expression patterns presented in Figure 8E. Importantly, according to cluster analysis, we could not identify a single gene which is missing from the exosome-related (i.e. exosome, $MSC^{PD\text{-}1+}$) groups in comparison to the control (i.e. non-exosome-related) tumor-bearing mice. In other words, whereas these exosome-related groups do exhibit such gene

expression profiles which are characteristics only to them, such individual profiles cannot be detected in the control group.

Specifically, the following gene expression patterns were defined:

- 3 genes (Elk1, Rb1, Igta2) were exclusively induced only in the exosome-treated group;
- 23 genes (Prom1, Tiam1, Bcl2, Bax, Casp9, Hgf, Jak2, Met, Mapk2k2, Alcam1, Eng, Flot2, Itga4, Itga6, Kit, Pecam1, Thy, Cdc42, Casp8, Ets1, Myb, Map2k1, Mapk1) were found to be upregulated both in the exosome and or $MSC^{PD\text{-}1+}$ cell treated groups;
- 14 genes (Bmi1, Cd44, Itgb1, Muc1, Cdk4, Nras, Sat3, Kitl, Raf1, Mtor, Akt1, Mapk3, Pik3ca, Rac1) were found to be upregulated in all three groups.

Finally, it should be noted that the dramatic gene expression alterations seen in the exosome-related (i.e. exosome, $MSC^{PD\text{-}1+}$) groups was exclusively due to the presence of the exosomes as the "$MSC^{PD\text{-}1+}$ only" cluster contained no genes (Figure 8F).

3.3. Identification of exosome-induced tumorigenic and cell survival signaling pathway(s)

In the *in vivo* expreiments, we detected overexpressed elements of 3 main pathways which do participate in tumor progression and metastasis formation. To demonstrate these results, and to explore the potential causative exosomal factors, we again performed an Ingenuity Pathway Analysis (IPA). A network was built from the overexpressed genes, and their complexes using the Path Explorer tool in the IPA Path Designer. Then a list was generated that contained the exosomal proteins detected by LC-MSMS (Table 1) and the exosomal miRNAs (Table 2) identified by SOLiD sequencing. The Grow tool in the IPA Path Designer revealed significant interactions between the expression network and the molecular content of these vesicles. The resulted interaction network (Figure 9) shows both direct and indirect interactions, but it contains only experimentally observed relationships based on the Ingenuity Knowledge Base. This network demonstrates that 61 types of exosomal molecules may affect tumor progression through pathways controlled by key components including MET, Ras, RAF1, Mek, ERK1/2, MITF, BCL2, PI3K, Akt, MTOR, PD-1, KIT, JAK STAT3 or ETS1.

Taken together, these findings demonstrate that interaction between exosomes and mesenchymal stem cells induce a tumor-like phenotype and PD-1 overexpression of naive cells *in vitro* and fast tumor progression *in vivo.*

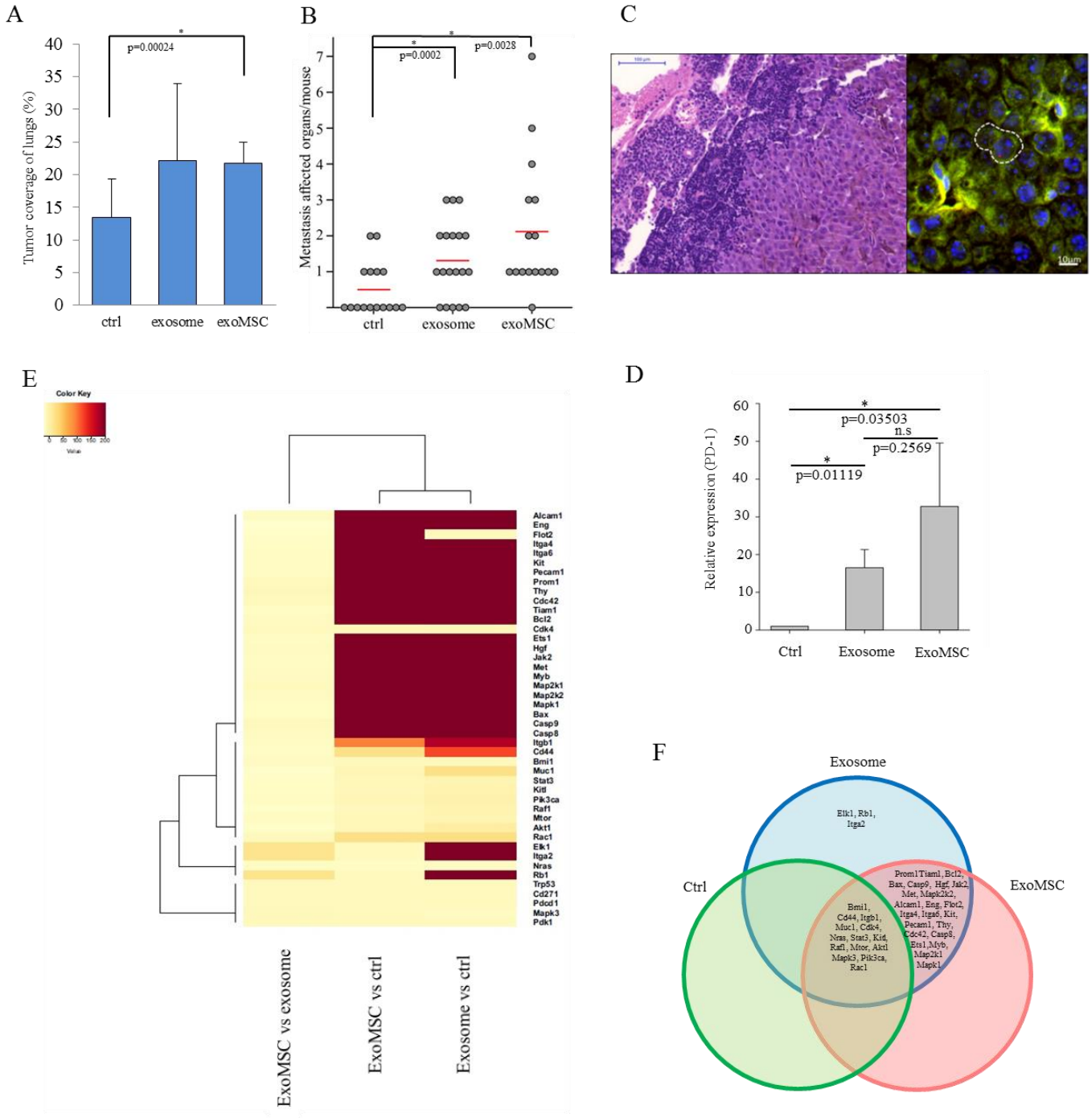

Figure 8. Melanoma exosomes promote tumor progression and metastasis formation *in vivo*

(A) Tumor coverage of lungs on day 15 in different animal groups. The graph represents mean + SD (n=3).

(B) Number of distant metasteses on day 25. One dot represents one animal in each group, red lines show the average number of metastases per animal.

(C) FISH analysis of a paraortic lymph node metastases, which showed the presence of exosome-exposed MSC. Y chromosome (red dot) of the male mouse-derived MSC was detected in the metastases of a female mouse.

(D) qRT-PCR analysis of PD-1 in the lung samples using TaqMan probes (n=3).

(E) Heatmap and cluster analysis of gene expression pattern, which show protooncogenic dominance in exosome or exoMSC groups. Robust hierarchical clustering based on fold changes in the gene expression data between selected groups divide the treated groups into several upper classes. Groups treated by exosomes or exoMSCs compared to untreated controls. Exosomes and exoMSC treatments were closely related.

(F) The Venn diagram shows all possible logical relations between a finite collections of different sets of genes were measured during gene expression profiling (see Figure 8E).

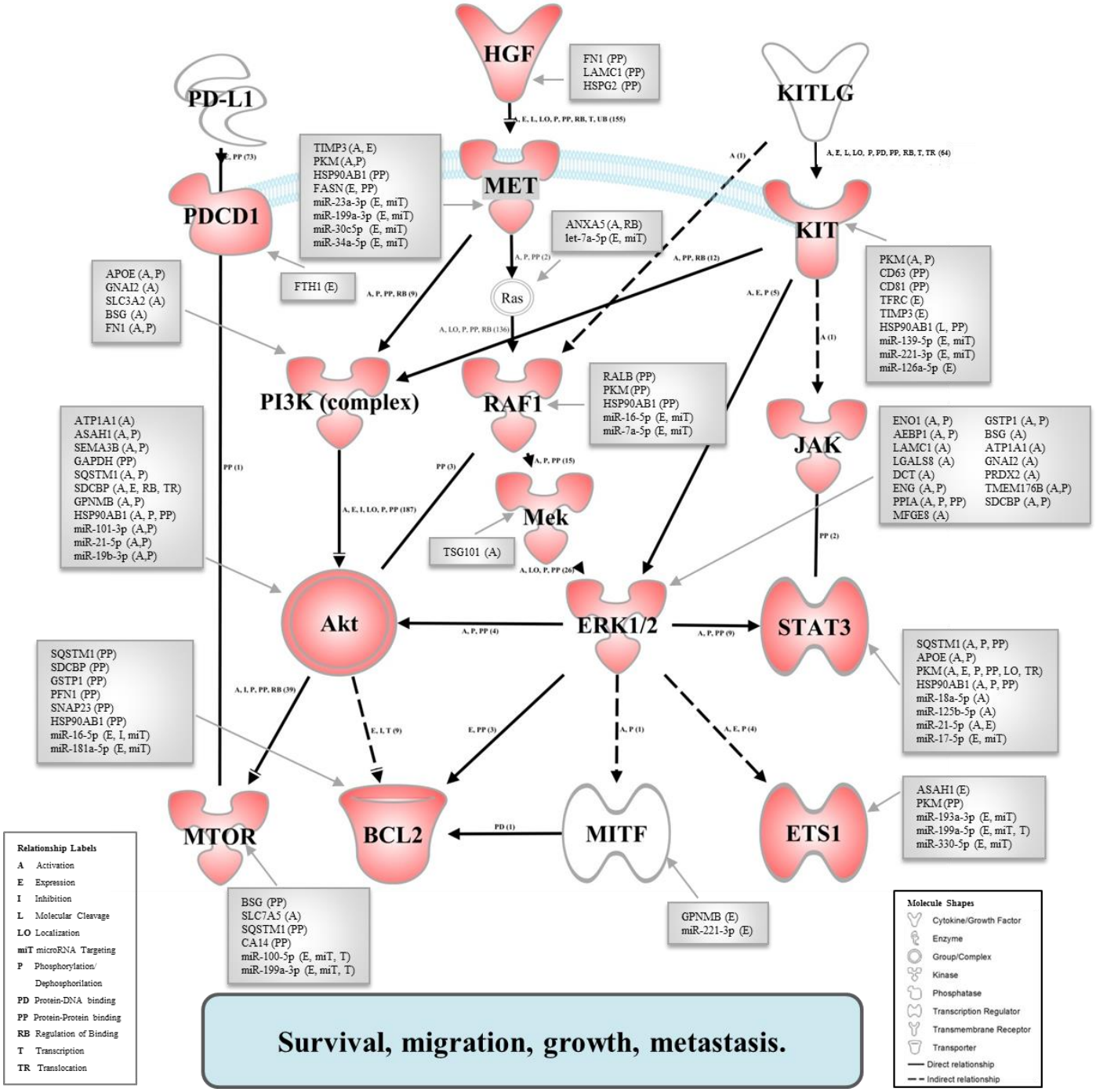

Figure 9. Integrated network of the *in vivo* overexpressed genes supplemented with the interacting exosomal factors.
The network of overexpressed genes (red symbols) was conceived by us based on literature data and the relationships between molecules were supported also by the IPA knowledge base. This was proven by the *in vivo* experiments (see Figure 8), where the tumor progression and the number of metastases were increased in the exosome-related goups. Network visualization was performed using the Path Explorer tool of the IPA Path Designer. The exosomal proteins and miRNAs (grey boxes) was connected to the network elements by the Grow tool of the IPA Path Designer based on experimentally proven data of the IPA knowledge base. Activation of the established network by exosomal components may support the survival, migration, growth and metastasis of tumor cells. Red symbols: gene products of *in vivo* overexpressed genes, white symbols: supplementary network elements, which were not investigated *in vivo*, grey boxes: interacting exosomal components (MET is double labelled with red and grey).

Planned dissemination of results 3.

"Our results will be presented at 1 national and 1 international scientific meeting. As the final step of our project we will write the second full paper and we expect to complete a thesis for a Ph. D. degree."

Accomplished dissemination of results 3.

In the 3rd year we published an original paper and presented our results in 1 international and 1 national conference. We had 3 other publications.

Publications:

1. Harmati M, Tarnai Z, Decsi G, Kormondi S, Szegletes Z, Janovak L, Dekany I, Saydam O, Gyukity-Sebestyen E, Dobra G, Nagy I, Nagy K, Buzas K.: Stressors alter intercellular communication and exosome profile of nasopharyngeal carcinoma cells., J Oral Pathol Med. J Oral Pathol Med. 2017 Apr;46(4):259-266.

Other publications:

1. Piccinini F, Balassa T, Szkalisity A, Molnar C, Paavolainen L, Kujala K, Buzas K, Sarazova M, Pietiainen V, Kutay U, Smith K, Horvath P.: Advanced Cell Classifier: User-Friendly Machine-Learning-Based Software for Discovering Phenotypes in High-Content Imaging Data., Cell Syst. 2017 Jun 28;4(6):651-655.e5.
2. Zsedenyi A, Farkas B, Abdelrasoul GN, Romano I, Gyukity-Sebestyen E, Nagy K, Harmati M, Dobra G, Kormondi S, Decsi G, Nemeth IB, Diaspro A, Brandi F, Beke S, Buzas K.: Gold nanoparticle-filled biodegradable photopolymer scaffolds induced muscle remodeling: in vitro and in vivo findings., Mater Sci Eng C Mater Biol Appl. 2017 Mar 1;72:625-630.

Oral presentations:

1. Edina Gyukity-Sebestyén, Mária Harmati, Gabriella Dobra, István B. Németh, Johanna Mihály, Ágnes Zvara, Éva Hunyadi-Gulyás, Róbert Katona, István Nagy, Péter Horváth, Tibor Pankotai, Miklós Erdélyi, Zoltán János Veréb, Lajos Kemény, Tamás Bíró, Krisztina Buzás. Intercellular communication between melanoma and stroma cells induce PD-1 overexpression and tumor progression. 6th Annual Meeting of the International Society for Extracellular Vesicles, Toronto, Canada, 2017.05.17-21.
2. Gyukity-Sebestyén Edina, Harmati Mária, Dobra Gabriella, Németh B. István, Mihály Johanna, Zvara Ágnes, Humyadi Gulyás Éva, Katona Róbert, Nagy István, Horváth Péter, Pankotai Tibor, Borsos Barbara, Veréb Zoltán János, Kemény Lajos, Bíró Tamás, Buzás Krisztina. Melanóma és sztróma sejtek közötti, onkoszómák mediálta intercelluláris kommunikáció PD-1 overexpressziót és tumorprogressziót eredményez. A Magyar Élettani Társaság, a Magyar Kísérletes és Klinikai Farmakológiai Társaság és a Magyar Mikrocirkulációs és Vaszkuláris Biológiai Társaság közös Vándorgyűlése, Debrecen, Hungary, 2017.06.13-16.

Two PhD degrees have been completed.

Annamária Marton, 2017

Ádám Zsedényi, 2018

Submitted: EDINA GYUKITY-SEBESTYÉN, MÁRIA HARMATI, GABRIELLA DOBRA, ISTVÁN B. NÉMETH, JOHANNA MIHÁLY, ÁGNES ZVARA, ÉVA HUNYADI-GULYÁS, RÓBERT KATONA, ISTVÁN NAGY, PÉTER HORVÁTH, ÁRPÁD BÁLIND, ÁBEL SZKALISITY, TIBOR PANKOTAI, BARBARA BORSOS, MIKLÓS ERDÉLYI, ZOLTÁN JÁNOS VERÉB, EDIT BUZÁS, LAJOS KEMÉNY, TAMÁS BÍRÓ, KRISZTINA BUZÁS
Melanoma-derived exosomes induce PD-1 overexpression and tumor progression via stem cell reprograming

References

Buzás K, Marton A, Vizler C, Gyukity-Sebestyén E, Harmati M, Nagy K, Zvara Á, Katona RL, Tubak V, Endrész V, Németh IB, Oláh J, Vígh L, Bíró T, Kemény L. Bacterial Sepsis Increases Survival in Metastatic Melanoma: Chlamydophila Pneumoniae Induces Macrophage Polarization and Tumor Regression. J Invest Dermatol. 2016;136(4):862-5. doi: 10.1016/j.jid.2015.12.032.

Karnoub AE, Dash AB, Vo AP, Sullivan A, Brooks MW, Bell GW, Richardson AL, Polyak K, Tubo R, Weinberg RA, Mesenchymal stem cells within tumour stroma promote breast cancer metastasis. Nature. 2007 Oct 4;449(7162):557-63.

Kleffel S, Posch C, Barthel SR, Mueller H, Schlapbach C, Guenova E, Elco CP, Lee N, Juneja VR, Zhan Q et al. (2015) Melanoma Cell-Intrinsic PD-1 Receptor Functions Promote Tumor Growth. Cell. 162(6):1242-56.

Liu HY, Chiou JF, Wu AT, Tsai CY, Leu JD, Ting LL, Wang MF, Chen HY, Lin CT, Williams DF, Deng WP. The effect of diminished osteogenic signals on reduced osteoporosis recovery in aged mice and the potential therapeutic use of adipose-derived stem cells.Biomaterials. 2012 Sep;33(26):6105-12. doi: 10.1016/j.biomaterials.2012.05.024. Epub 2012 Jun 12.

Lötvall J, Hill AF, Hochberg F, Buzás EI, Di Vizio D, Gardiner C, Gho YS, Kurochkin IV, Mathivanan S9, Quesenberry P, Sahoo S, Tahara H, Wauben MH, Witwer KW, Théry C. Minimal experimental requirements for definition of extracellular vesicles and their functions: a position statement from the International Society for Extracellular Vesicles. J Extracell Vesicles. 2014 Dec 22;3:26913. doi: 10.3402/jev.v3.26913. eCollection 2014.

Peinado H, Alečković M, Lavotshkin S, Matei I, Costa-Silva B, Moreno-Bueno G, Hergueta-Redondo M, Williams C, García-Santos G, Ghajar C, Nitadori-Hoshino A, Hoffman C, Badal K, Garcia BA, Callahan MK, Yuan J, Martins VR, Skog J, Kaplan RN, Brady MS, Wolchok JD, Chapman PB, Kang Y, Bromberg J, Lyden D. Melanoma exosomes educate bone marrow progenitor cells toward a pro-metastatic phenotype through MET. Nat Med. 2012 Jun;18(6):883-91. doi: 10.1038/nm.2753.

Yáñez-Mó M, Siljander PR, Andreu Z, Zavec AB, Borràs FE, Buzas EI, Buzas K, Casal E, Cappello F, Carvalho J et al. (2015). Biological properties of extracellular vesicles and their physiological functions. J Extracell Vesicles. 4: 10.3402/jev.v4.27066.

References of Table 3:

T 1. Nie G, Duan H, Li X, et al. MicroRNA-205 promotes the tumorigenesis of nasopharyngeal carcinoma through targeting tumor protein p53-inducible nuclear protein 1. Mol Med Rep 2015; 12(4): 5715-22.

T2. Qu C, Liang Z, Huang J, et al. MiR-205 determines the radioresistance of human nasopharyngeal carcinoma by directlytargeting PTEN. Cell Cycle 2012; 11(4): 785-96.

T3. Wong TS, Man OY, Tsang CM, et al. MicroRNA let-7 suppresses nasopharyngeal carcinoma cells proliferation throughdownregulating c-Myc expression. J Cancer Res Clin Oncol 2011; 137(3): 415-22.

T4. Ou H, Li Y, Kang M. Activation of miR-21 by STAT3 induces proliferation and suppresses apoptosis in nasopharyngeal carcinoma by targeting PTEN gene. PLoS One 2014; 9(11): e109929.

T5. Li Y, Yan L, Zhang W, et al. miR-21 inhibitor suppresses proliferation and migration of nasopharyngeal carcinoma cells through down-regulation of BCL2 expression. Int J Clin Exp Pathol 2014; 7(6): 3478-87.

T6. Yang GD, Huang TJ, Peng LX, et al. Epstein-Barr Virus_Encoded LMP1 upregulates microRNA-21 to promote the resistance ofnasopharyngeal carcinoma cells to cisplatin-induced Apoptosis by suppressing PDCD4 and Fas-L. PLoS One 2013; 8(10): e78355.

T7. Wu Z-s, Wu Q, Wang C-q, et al. MiR-339-5p inhibits breast cancer cell migration and invasion in vitro and may be a potential biomarker for breast cancer prognosis. BMC Cancer 2010; 10: 542.

T8. Zhou C, Liu G, Wang L, et al. MiR-339-5p regulates the growth, colony formation and metastasis of colorectal cancer cells by targeting PRL-1. PLoS One 2013; 8(5): e63142.

T9. Li Y, Zhao W, Bao P, et al. miR 339 5p inhibits cell migration and invasion in vitro and may be associated with the tumor node metastasis staging and lymph node metastasis of non small cell lung cancer. Oncol Lett 2014; 8(2): 719-725.

T10. Süslüer SY, Biray Avci Ç, Şiğva ZÖD, et al. Detection of miRNA Expression Alteration in Diffuse and High Grade Glial Tumors. J Neurol Sci 2015; 32(1), 64-88.

T11. Khan FH, Pandian V, Ramraj S, Aravindan S, Herman TS, Aravindan N. Reorganization of metastamiRs in the evolution of metastatic aggressive neuroblastoma cells. BMC Genomics 2015; 16(1): 501.

T12. Xu HS, Zong HL, Shang M, et al. MiR-324-5p inhibits proliferation of glioma by target regulation of GLI1. Eur Rev Med Pharmacol Sci 2014; 18(6): 828-32.

T13. Lyu X, Fang W, Cai L, et al. TGFβR2 is a major target of miR-93 in nasopharyngeal carcinoma aggressiveness. Mol Cancer 2014; 13: 51.

T14. Hirata H, Hinoda Y, Shahryari V, et al. Genistein downregulates onco-miR-1260b and upregulates sFRP1 and Smad4 via demethylation and histone modification in prostate cancer cells. Br J Cancer 2014; 110(6): 1645-54.

T15. Liao W, Gu C, Huang A, Yao J, Sun R. MicroRNA-33b inhibits tumor cell growth and is associated with prognosis in colorectal cancer patients. Clin Transl Oncol (in press).

T16. Xu N, Li Z, Yu Z, et al. MicroRNA-33b suppresses migration and invasion by targeting c-Myc in osteosarcoma cells. PLoS One 2014; 9(12): e115300.

T17. Lin J, Huang S, Wu S, et al. MicroRNA-423 promotes cell growth and regulates G(1)/S transition by targeting p21Cip1/Waf1 in hepatocellular carcinoma. Carcinogenesis 2011; 32(11): 1641-7.

T18. Kitago M, Martinez SR, Nakamura T, Sim MS, Hoon DS. Regulation of RUNX3 tumor suppressor gene expression in cutaneous melanoma. Clin Cancer Res 2009; 15(9): 2988-94.

T19. Yang F, Nam S, Brown CE, et al. A novel berbamine derivative inhibits cell viability and induces apoptosis in cancer stem-like cells of human glioblastoma, via up-regulation of miRNA-4284 and JNK/AP-1 signaling. PLoS One 2014; 9(4): e94443.

T20. Chen Z, Jin Y, Yu D, et al. Down-regulation of the microRNA-99 family members in head and neck squamous cell carcinoma. Oral Oncol 2012; 48(8): 686-91.

T21. Kang J, Lee S, Lee S, et al. microRNA-99b acts as a tumor suppressor in non-small cell lung cancer by directly targeting fibroblast growth factor receptor 3. Exp Ther Med 2012; 3(1): 149-153.

22. Sun D, Lee YS, Malhotra A, et al. miR-99 family of MicroRNAs suppresses the expression of prostate-specific antigen and prostate cancer cell proliferation. Cancer Res 2011; 71(4): 1313-24.

T23. Tang R, Qi Q, Wu R, et al. The polymorphic terminal-loop of pre-miR-1307 binding with MBNL1 contributes to colorectal carcinogenesis via interference with Dicer1 recruitment. Carcinogenesis. 2015; 36(8): 867-75.

T24. Liu N, Jiang N, Guo R, et al. MiR-451 inhibits cell growth and invasion by targeting MIF and is associated with survival in nasopharyngeal carcinoma. Mol Cancer 2013; 12(1): 123.

T25. Fukumoto I, Kinoshita T, Hanazawa T, et al. Identification of tumour suppressive microRNA-451a in hypopharyngeal squamous cell carcinoma based on microRNA expression signature. Br J Cancer 2014; 111(2): 386-94.

T26. Kuo PL, Liao SH, Hung JY, Huang MS, Hsu YL. MicroRNA-33a functions as a bone metastasis suppressor in lung cancer by targeting parathyroid hormone related protein. Biochim Biophys Acta 2013; 1830(6): 3756-66.

T27. Zhu J, Chen L, Zou L et al. MiR-20b, -21, and -130b inhibit PTEN expression resulting in B7-H1 over-expression in advanced colorectal cancer. Hum Immunol 2014; 75(4): 348-53.

T28. Lai KW, Koh KX, Loh M, et al. MicroRNA-130b regulates the tumour suppressor RUNX3 in gastric cancer. Eur J Cancer 2010; 46(8): 1456-63.

T29. Zhao G, Zhang J-g, Shi Y, et al. MiR-130b Is a Prognostic Marker and Inhibits Cell Proliferation and Invasion in Pancreatic Cancer through Targeting STAT3. PLoS One 2013; 8(9): e73803.

T30. Zhang C, Fang X, Li W, et al. Influence of recombinant lentiviral vector encoding miR-15a/16-1 in biological features of human nasopharyngeal carcinoma CNE-2Z cells. Cancer Biother Radiopharm 2014; 29(10): 422-7.

T31. Zhu JY, Pfuhl T, Motsch N, et al. Identification of novel Epstein-Barr virus microRNA genes from nasopharyngeal carcinomas. J Virol 2009; 83(7): 3333-41.

T32. Yao K, He L, Gan Y, Zeng Q, Dai Y, Tan J. MiR-186 suppresses the growth and metastasis of bladder cancer by targeting NSBP1. Diagn Pathol 2015; 10: 146.

T33. Cui G, Cui M, Li Y, et al. MiR-186 targets ROCK1 to suppress the growth and metastasis of NSCLC cells. Tumour Biol 2014; 35(9): 8933-7.

T34. Ji Y, He Y, Liu L, Chong X. MiRNA-26b regulates the expression of cyclooxygenase-2 in desferrioxamine-treated CNE cells. FEBS Lett 2010; 584(5): 961-7.

T35. Cui R, Kim T, Fassan M, et al. MicroRNA-224 is implicated in lung cancer pathogenesis through targeting caspase-3 and caspase-7. Oncotarget 2015; 6(26): 21802-15.

T36. He X, Zhang Z, Li M, et al. Expression and role of oncogenic miRNA-224 in esophageal squamous cell carcinoma. BMC Cancer 2015; 15(1): 575.

T37. Cheung CC, Chung GT, Lun SW, et al. miR-31 is consistently inactivated in EBV-associated nasopharyngeal carcinoma andcontributes to its tumorigenesis. Mol Cancer 2014; 13: 184.

T38. Lou F, Ma HN, Xu L Chen M, Zhu YB. Two polymorphisms of CD44 3'UTR weaken the binding of miRNAs and associate with naso-pharyngeal carcinoma in a Chinese population. Eur Rev Med Pharmacol Sci 2014;18(17):2444-52.